AFIT/GAP/ENP/95D-09

PHOTOLUMINESCENCE AND ELECTROLUMINESCENCE OF ERBIUM AND NEODYMIUM IMPLANTED SEMICONDUCTORS

THESIS

James R. Hunter, B.S.
First Lieutenant, USAF

AFIT/GAP/ENP/95D-09

19960118 034

AFIT/GAP/ENP/95D-09

PHOTOLUMINESCENCE AND ELECTROLUMINESCENCE OF ERBIUM AND NEODYMIUM IMPLANTED SEMICONDUCTORS

THESIS

Presented to the Faculty of the Graduate School of Engineering
of the Air Force Institute of Technology
Air University
in Partial Fulfillment of the
Requirements for the Degree of
Master of Science in Engineering Physics

James R. Hunter, B.S.
First Lieutenant, USAF

December 1995

AFIT/GAP/ENP/95D-09

PHOTOLUMINESCENCE AND ELECTROLUMINESCENCE OF ERBIUM AND NEODYMIUM IMPLANTED SEMICONDUCTORS

James R. Hunter, B.S.
1st Lieutenant, USAF

Approved:

Robert L Hengehold 29 Nov '95
Robert L. Hengehold
Chairman, Advisory Committee

Yung Kee Yeo 27 Nov '95
Yung Kee Yeo
Member, Advisory Committee

Paul H. Ostdiek 29 Nov '95
Paul H. Ostdiek, Lieutenant Colonel, USAF
Member Advisory Committee

Acknowledgments

Primarily, I would like thank Greg Smith for spending all those hours helping me set up the equipment and for providing assistance throughout the never-ending cycle of equipment breakdowns. I would not have been able to complete this work without his guidance as to what will and will not break the equipment and for providing periodic sanity checks when the data is not as it should be (yes, the entrance slit is now open!). Belinda Johnson also deserves a pat on the back for her expedient lithography processing and valuable information as to what chemicals are good for what processes.

I would also like to thank my advisors, Dr. Robert Hengehold and Dr. Yung Kee Yeo, for making sure materials and processing procedures were made available to me throughout the thesis period and for providing insight into the physics of what results were observed.

Thanks also to doctoral candidate Eric Silkowski for providing valuable advice on equipment procedures and different parts of solid-state theory and also for filling my LN_2 dewar when I wasn't around.

Universal Energy Systems deserves credit for the timely job of performing the actual ion implantation. Finally, I would like thank Wright Laboratories for the use of their clean room in which the lithography was done and for their speedy diode packaging.

James R. Hunter

Table of Contents

Page

List of Figures

List of Tables

Abstract

Low temperature photoluminescence (PL) and electroluminescence (EL) measurements were used to study the excitation of erbium- and neodymium-implanted GaAs and $Al_xGa_{1-x}As$ (x=0.1, 0.3) pn-junctions. The rare-earth (RE) emissions were investigated as a function of ion dose, aluminum mole fraction, laser excitation power, and applied forward bias voltage for the implanted samples. Low temperature PL was also measured from Er doped silicon grown by the metalorganic chemical vapor-phase deposition (MOCVD) method using various growth parameters.. The MOCVD-grown Si samples were studied as a function of metalorganic source temperature, silane (SiH_4) flow, growth time, and hydrogen presence during growth. PL peaks, observed near 1.54 μm for Er-implanted GaAs and $Al_xGa_{1-x}As$ and Er-doped Si, and near 1.11 μm for Nd-implanted samples, can be attributed to the crystal-field-split spin-orbit transitions of $^4I_{13/2}\rightarrow^4I_{15/2}$ and $^4F_{3/2}\rightarrow^4I_{9/2}$, respectively. Photoluminescence of the ion-implanted pn-junctions revealed that the luminescent intensity is highest, and increases with dose when the Er^{3+} peak concentration falls in the p-type region, but PL of the Nd^{3+} demonstrated only a slight preference for the n-type region. The luminescent signal is much stronger for an aluminum mole fraction of 0.1 than for 0.3. Observed for the first time, to the best of our knowledge, was Nd^{3+} electroluminescence at ~1.11 μm from pn- and np- junctions having a dose of 1×10^{13} cm^{-2}. The strongest PL peaks located near the 1.54 μm were observed in the Si:Er when a high flow rate of silane (5.0 sccm) and a longer growth time (70 min) were utilized in the factorial study of the MOCVD samples grown at 5 mTorr with a substrate temperature of 420 °C.

PHOTOLUMINESCENCE AND
ELECTROLUMINESCENCE OF ERBIUM
AND NEODYMIUM IMPLANTED SEMICONDUCTORS

I. Introduction

The rare-earths (RE), those elements numbered fifty-eight through seventy-one in the periodic table of elements, have enjoyed increased popularity due to the nature of their optical properties. The unique property of the RE atom is that the outer shell electrons shield the partially filled 4f-shell from the host lattice's crystal field and temperature effects. As a result, a relatively narrow, spectrally unshifted peak is the signature of an intra-4f emission. The importance of this characteristic can be realized in producing solid state optoelectronic devices, such as narrow-band light emitting diodes or diode lasers. As an example, erbium intra-4f-shell transitions yield a luminescent peak near 1.54 μm ($^4I_{13/2} \rightarrow {}^4I_{15/2}$), which is the wavelength where the least amount of attenuation in silica based fiber optics occurs. If one were able to fabricate a high efficiency device capable of emitting a burst of sufficiently high intensity at this wavelength, the amount of applied photonics seen in industry would take a giant leap forward. The Air Force could benefit from this explosion immensely. Because the RE emissions show very little spectral shift over a range of temperatures, photonic circuits could be placed in higher temperature environments, such as closer to jet engines, and not suffer from signal loss due to temperature caused spectral line shifts. Aircraft weight could be cut down by using fiberoptic cable, instead of wire, connected to a GaAs:Er^{3+} controller device. And with a lighter aircraft, the resulting savings the Air Force and the other service branches in fuel alone could potentially be quite vast.

However, most previous studies on REs in semiconductors have been in the area of photoluminescence (PL). The resulting shortfall in information on observed electroluminescence (EL) in the REs has left this area ripe for research. The goal of this investigation is to study low temperature PL and EL of the rare-earths erbium, which has its strongest intensity peak at the $^4I_{13/2} \rightarrow ^4I_{15/2}$ transition, and neodymium, which has its strongest intensity peak at the $^4F_{3/2} \rightarrow ^4I_{9/2}$ transition. In order to better understand the nature of the EL observed, PL measurements were taken on the same sample groups and compared.

Very little has been documented regarding EL of Er-implanted III-V semiconductors and even less for Nd. In one study, Klein et al. (1) demonstrated Er EL despite the fact that they expected freeze-out of the dopant at 4 K. In another study, Chang and Takahei also demonstrated forward and reverse biased Er EL of Metalorganic Chemical Vapor-phase Deposition (MOCVD)-grown GaAs (2). However, EL of ion-implanted $Al_xGa_{1-x}As$ has not been reported.

In this study, EL and PL measurements were performed on Er and Nd implanted $Al_xGa_{1-x}As$ (x=0.1, 0.3) pn-junctions and GaAs pn- and np- junctions. In addition, PL measurements were made on Er doped silicon. The University of Vermont provided the erbium-doped MOCVD-grown silicon samples which were measured as part of a MOCVD growth-method comparison. The GaAs and $Al_xGa_{1-x}As$ samples were ion implanted at an ion energy required to put the peak concentration at the pn- interface with

Er and Nd ion doses of both 1×10^{13} and 5×10^{13} cm^{-2}. The Rapid Thermal Annealing (RTA) process was used to anneal the samples at 750 °C.

The first part of the experimental process consisted of measuring the PL of the erbium doped silicon (Si:Er). This data provided a comparative baseline of luminescent intensity since it was the combination which has been most thoroughly investigated and, hence, more thoroughly understood, for example Namavar successfully fabricated a room temperature Si:Er light emitting diode (3). Once that was accomplished, the photoluminescence of the GaAs and $Al_xGa_{1-x}As$ diodes was obtained to establish a base of luminescent intensity for the pn- and np-junctions against which the EL data could be compared. Previous studies have shown that the luminescent intensity resulting from optical excitation of RE doped GaAs and $Al_xGa_{1-x}As$, n- or p-type, compounds are too low to show promise for optoelectronic devices (4). The EL of rare-earth implanted devices has been shown from previous studies to produce even lower intensities and thus even less promise (1). This phenomenon could possibly be explained in part by the fact that it has only been within the past few years that thorough studies have been completed which determine the optimum fabrication conditions for obtaining maximum PL signal strength from rare-earth implanted III-V semiconductors. Building on these results, it may now be possible to develop a diode with sufficient luminescent signal for use in an electrically driven device.

This thesis is broken into five major chapters. After this brief introductory chapter, Chapter II will give a short synopsis of the semiconductor physics that describe the luminescence under observation as well as an overview of previous photoluminescence work done with rare-earth implanted III-V compounds. Chapter III describes the experimental apparatus used for each characterization method, response of the apparatus, and general procedures for obtaining spectra from the samples in question. Analysis of the spectra will be covered in Chapter IV. The first part of Chapter IV will present the results of the Si:Er from the University of Vermont along with a discussion of which MOCVD growth method produced the best results. Differences in luminescent signal related to differing doses in the pn- and np-GaAs and pn-$Al_xGa_{1-x}As$ will be discussed in second part of Chapter IV. The effects of different mole fractions in the $Al_xGa_{1-x}As$ will be covered towards the end of Chapter IV. The end of Chapter IV discusses the results of the electroluminescence measurements of the erbium and neodymium-implanted GaAs and $Al_xGa_{1-x}As$. Lastly, a summary of experimental results will be given in Chapter V as well as possible directions for future research in achieving the goal of a viable rare-earth implanted electroluminescent device.

II. Background and Theory

Semiconductors and Band Theory

There are three main classes of materials relevant to electronic devices. These are conductors, insulators, and semiconductors. Conductors have partially filled conduction bands and, therefore, conduct even at low temperatures. An Insulator's conduction bands are completely filled at low temperatures. Since they have a relatively large band gap, they remain nonconducting even above room temperature, however, when raised to high enough temperatures they will eventually conduct. The last class to be considered is the semiconductor and it displays some interesting characteristics.

Semiconductors are insulators near zero degrees Kelvin, but when heated sufficiently, electrons can overcome the bandgap. Therefore, semiconductors start to conduct at much lower temperatures than insulators. However, when the right impurity is found in the lattice structure of a semiconductor the conductivity can rise (this is not true in all cases; a Zn implant can make n-type GaN an insulator). This phenomenon can be explained by the band theory of solids. Atoms in a semiconductor lattice have wavefunctions that overlap and form quasi-continuous bands of allowed electronic energy states. These allowed bands are separated by a forbidden band, called the bandgap. Near zero Kelvin, the so called valence band is completely filled. When the lattice temperature is raised, the wavefunction's thermal energy can allow electrons to gain enough energy to overcome the forbidden gap and occupy the so-called conduction band. Impurities often form energy states within the forbidden band. The thermal energy necessary for an impurity to overcome the separation of the nearest band is much smaller than the energy required for an electron in the valence band to overcome the bandgap energy and make a transition into the conduction band. At low temperatures the electrons fill the allowed energy bands from the lowest energy to the highest energy. The band structure for conductors, insulators, and semiconductors (both doped and undoped) is presented in Figure 1.

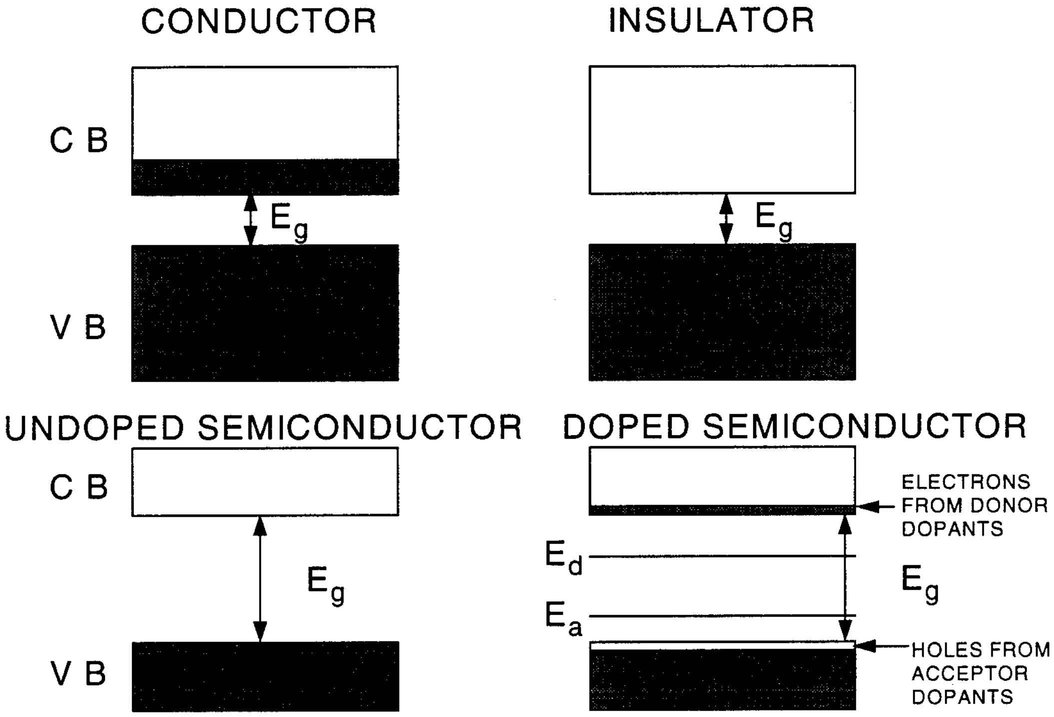

Figure 1. Band diagrams of conductors, insulators, and undoped and doped semiconductors at low temperatures.

When an allowed band is completely filled or completely empty it will not conduct. For a higher temperature, the electrons in a particular band (usually the topmost band) will gain enough energy to jump up to the next highest band across the energy gap leaving a hole behind (5 :458-464). A hole is an absence of an electron and is treated like a positively charged electron. With electron-hole pairs now created, the conductivity of the material will start to rise, increasing with the growing number of electron-hole pairs.

With a semiconductor at a low enough temperature, all the lower electron energy states of the valence band will be filled. When an applied voltage or incident photon hits the material with sufficient energy an electron will transition to the next higher band and leave a hole in the lower energy state. When an electron-hole pair binds together via Coulombic forces it is called an exciton. Once the exciton is formed, several different things can now occur. The exciton's electron and hole can recombine with the energy going into the lattice, the energy can be given to another electron in an Auger process, the electron and hole can recombine to emit a photon, or a combination of these processes can occur in series. These emitted photons are what is detected in the PL and EL processes.

Impurities in the Lattice

Now that the basics of band structure have been explained, we look at the impurities and the particular lattices into which the impurities were injected. This work focused on two main lattice types. For silicon, the lattice structure is of the diamond type, for GaAs and $Al_xGa_{1-x}As$ it is zincblende or sphalerite. These lattices are shown in Figure 2 (6 :10,12). The shaded atoms in (b) indicate where the Ga and Al atoms are placed and the clear atoms show As placement. The dashed lines in both diagrams define the lattice basis cell and the parameter "a" is the unit cell edge length.

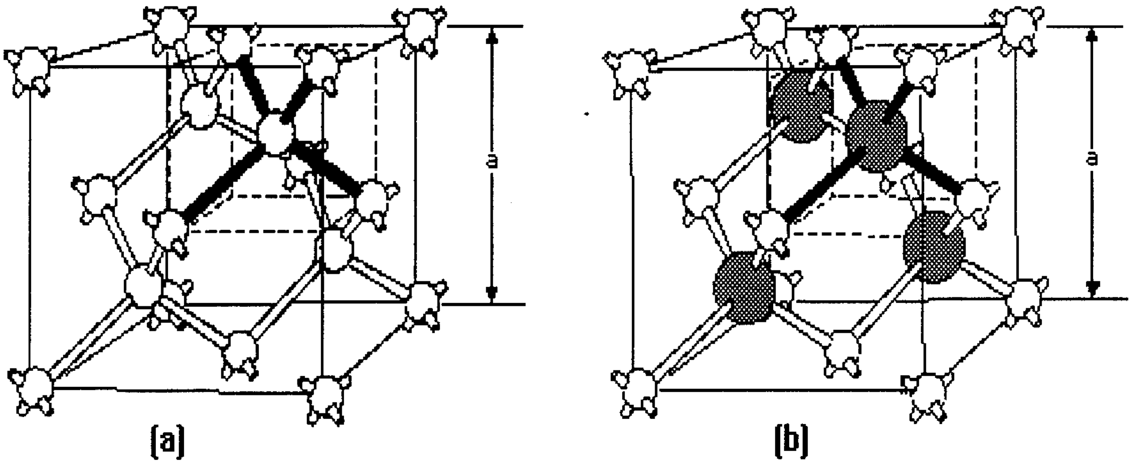

Figure 2. The lattice structure for (a) silicon and (b) GaAs and $Al_xGa_{1-x}As$.

As Figure 2 shows, the two lattice types are identical in form with the difference between them being that the diamond lattice is composed entirely of silicon atoms and the zincblende lattice is composed of two or more types of atoms (in this case Ga, As, and Al). With $Al_xGa_{1-x}As$, the Al replaces some of the Ga atoms. With this in mind, we can look at the effect of impurities such as the addition of a rare-earth ion to the lattice. The position of a particular rare-earth impurity, such as Er or Nd, in the lattice can be classified as either an interstitial site, i.e. occupies one of the empty spaces in the lattice, or a substitutional site, replaces a lattice atom. In most cases, the REs will be found on both interstitial and substitutional sites. Impurities are not likely to be found along a host lattice bond, since this would mean an unstable energy state resulting from a repulsive Coulombic potential. Where these impurities reside depends on the growth process of the lattice, in the case of silicon, or implantation of the impurities and subsequent annealing conditions of the lattice in the case of GaAs and $Al_xGa_{1-x}As$. Takahei, Taguchi, and Horikoshi have found in their work with Er implanted GaAs that the intensity of the luminescence depends on the concentration of the RE^{3+} ions residing in the zincblende lattice's tetragonal interstitial sites rather than on the concentration at substitutional sites (7).

Metalorganic Chemical Vapor-phase Deposition

The MOCVD method of growth incorporates impurities during the growth of the lattice. The basic procedure for the MOCVD process using silicon as the host lattice is to flow a metalorganic gas and silane (SiH_4) over a hot substrate surface. The hot substrate accumulates Si:Er layers by breaking the molecular bonds of the metalorganic gas and silane. Once the bonds are broken, the metal and silicon fall to the substrate and the residual gas is pumped out of the chamber. For the MOCVD-grown samples used in this study, the sample chamber was held at 5 mTorr and the metalorganic used with the silane was composed of tri-(bis dimethyl silyl amido) Er.

The result of such a growth process leads to a more uniform distribution of the Er^{3+} ions in desired positions in the lattice and less lattice defects compared to other techniques, such as ion implantation. The resulting material can be used as-is or further processing, such as annealing, can be performed to optimize the erbium signal for luminescent studies. The Si:Er samples studied in this thesis were prepared by MOCVD by Professor W. Varhue at the University of Vermont (8)

Ion Implantation

In order to incorporate the REs into GaAs and $Al_xGa_{1-x}As$ host lattices, ion implantation was used. Ion implantation takes a RE source and energizes it, usually by heating, causing dislocations, and then accelerates the dissociated atoms by an electric field into the surface of the host material with sufficient energy to embed the atom at a precalculated depth in the material. In this study, the depth to which the atoms where implanted was roughly the depth of the interface of the p and n host materials. Table 1. gives the ion, energy and calculated depth of the ion implants. The depth calculations were performed using the Ion Beam Profile Code software, version 2.1 by Implant Sciences Corp.(9). The host materials themselves, GaAs and $Al_xGa_{1-x}As$, where grown by the Liquid Encapsulated Czochralaski/Vertical Gradient Freeze (LEC/VGF) process. This method incorporates silicon and carbon into the resulting n- and p-type layers of the material, respectively, as it is grown in order to form the pn-junction of the final luminescent devices.

Table 1.
Ion implantation depths and energies.

	Erbium			Neodymium		
Host Material	Implant Energy	Peak Concentration Depth (Å)	Straggling (Å)	Implant Energy	Peak Concentration Depth (Å)	Straggling (Å)
np-GaAs	1150	2096.9	593.2	910	2619.4	809.3
pn-GaAs	1150	2096.9	593.2	910	2619.4	809.3
pn-$Al_{.1}Ga_{.9}As$	1150	2123.3	595.4	910	2653.6	812.6
pn-$Al_{.3}Ga_{.7}As$	1150	2228.0	613.0	910	2787.6	837.4

A major drawback of the ion implantation process is that it introduces severe lattice damage to the host material which can quench the desired RE luminescence. In order to repair the lattice, annealing must be performed. Kozanecki et al (10) found that after implantation in GaAs, most Er^{3+} ions occupy interstitial sites. Annealing moved these ions to substitutional Ga sites, but in the process optical activity decreased. In one study by Elsaesser et al. (11), the optimum peak heights obtained for Nd and Er dopants in plain GaAs and $Al_xGa_{1-x}As$ occurred when the Rapid Thermal Annealing (RTA) process was used. The study determined that the best temperature for RTA is 750 °C with an optimized dose of 5×10^{13} cm^{-2} for both Er and Nd. Results of these studies show that that there is a target concentration of RE ions in interstitial sites. One point to remember, however, is that these results were for n-, p-, or semi-insulating host lattices, not for pn-junctions. The question of whether there might be a better annealing temperature for GaAs and $Al_xGa_{1-x}As$ pn- and np-junctions is a direction for future research.

Luminescence of the Rare-earths

There are only a discrete number of energy levels in any atom that an electron can jump up into before it decays back down to its unexcited state. These states are dictated by quantum mechanical selection rules. Since the REs are shielded from the crystal field by the outer shell electrons, the selection rules of a free ion should still apply (12 :333). The resulting allowed energy levels for trivalent rare-earth ions in $LaCl_3$ are shown in Figure 3 (13 :14). The actual placement of the RE energy levels with respect to the host GaAs or AlGaAs is unknown. Figure 4 shows a possible placement of the energy levels of Er^{3+} (a similar diagram could be drawn for Nd^{3+} in GaAs and AlGaAs as well) (14 :15). Note that the width is of the energy levels is larger in the Er^{3+} than the host bandgap.

With this understanding of the structure of the actual samples used, we now look to the processes used to measure the luminescent properties of the REs. Analyzing the luminescence from RE transitions is performed with a monochromator which can distinguish which wavelength was emitted. This process is the crux of the research at hand. The impurity and lattice will be energized from its thermal equilibrium energy state and the output of the decay processes will be measured and analyzed. The two analytical methods that were utilized in this study were photoluminescence and electroluminescence.

Figure 3. Allowed energy levels for trivalent rare-earths in a LaCl host lattice.

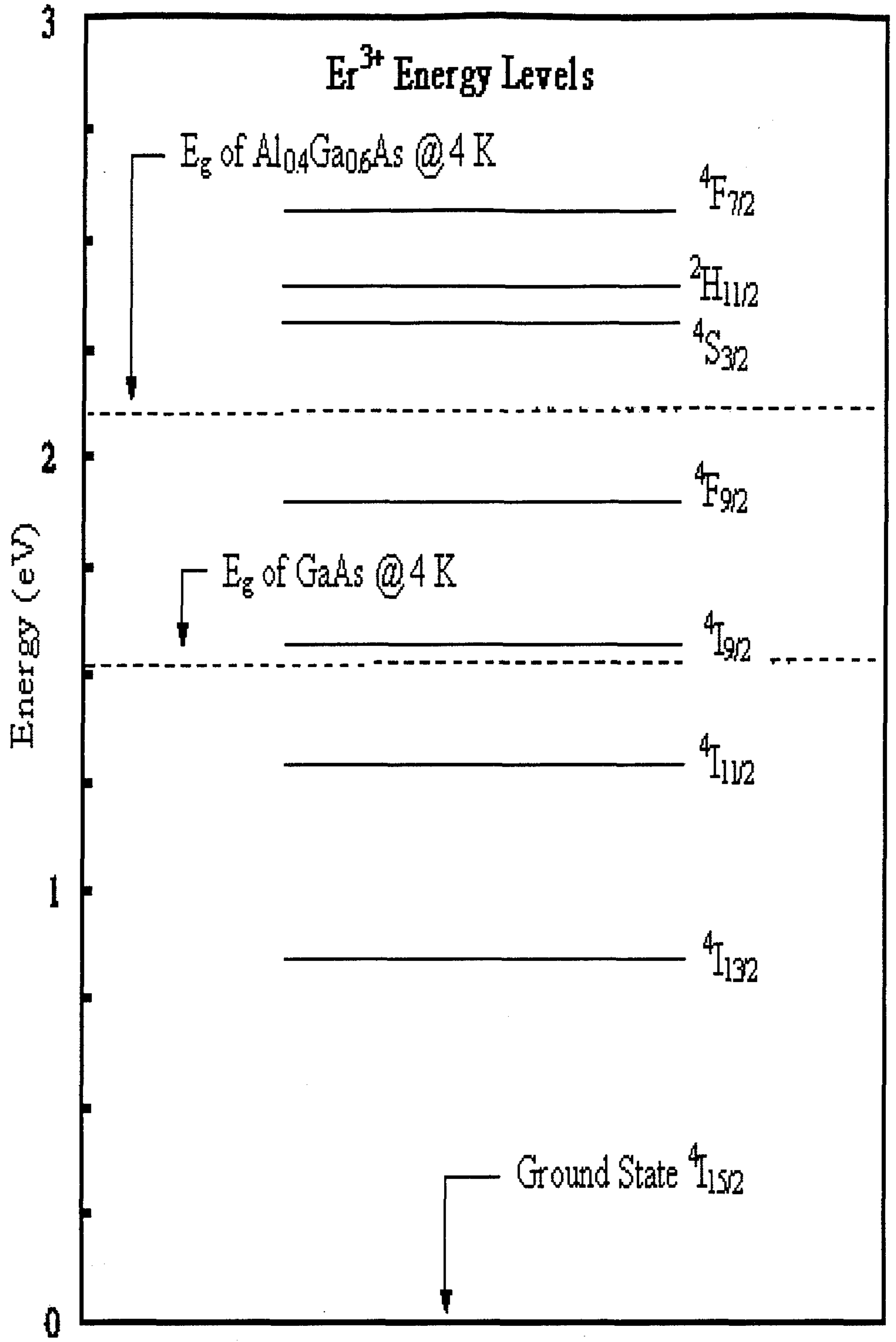

Figure 4. Relative positions of the spin-orbit crystal field split energy levels of Er^{3+} and host material bandgaps.

Photoluminescence

Photoluminescence was the first method used to obtain spectra from RE emissions. One advantage of PL is that sample preparation is less time consuming. Samples for PL were ready for measurement right after the host material was cut into small enough pieces (¼" × ¼"). Even the samples that were ion implanted only required two extra steps (implantation and annealing) before they were ready for measurement.

The physics involved in the excitation of the Er^{3+} ion in Si and III-V compounds is only now beginning to be understood (15), while Nd^{3+} in the same host materials has almost been neglected. However, some success has been seen in Nd doped materials by Nakagome and Takahei (16). The photo-excitation of these ions can happen directly and indirectly through the excitation of outer shells.

Electroluminescence

EL studies require more complex fabrication of the samples. Sample preparation for this procedure now involves use of mesa diode lithography which will be outlined in Chapter III. In EL, a voltage is applied to a pn-junction which effectively alters the alignment of the band structures of the two materials. At the interface of the two materials, some of the electrons from the n-type material travel into the p-type material and fill the holes they find there, causing a region with neutral charge or a "depletion region." Under unbiased conditions, or thermal equilibrium conditions, the energy band structure looks like Figure 5(a) (17 :71) and (18 :179).

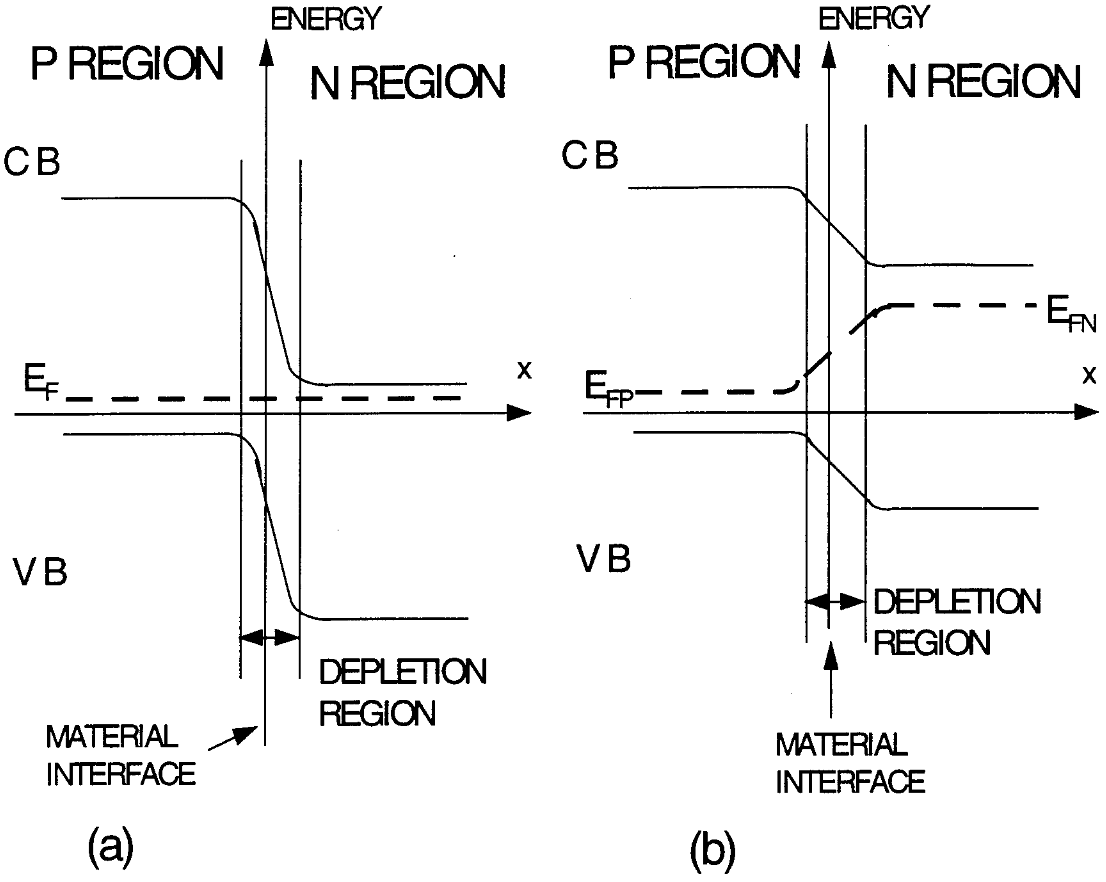

Figure 5. Energy bands at a pn-junction under (a) thermal equilibrium and (b) a forward bias.

When forward biased as in Figure 5(b), the p-type region's holes recombine with injected electrons and the width of depletion region is reduced. As a result, the n-type region's band structure effectively shifts upward. With enough applied forward bias, the electrons in the conduction band and the holes in the valence band are able to overcome the energy barrier of the depletion region and flow to the opposite side of the junction. The exact nature of the RE excitation is unknown at this time since the exact relative position of the RE^{3+} energy levels is unknown. From Figure 3, one sees that any number of excitation mechanisms could be possible. Some work has been done in trying to ascertain the energy level positions by Thee and Colon but much uncertainty still remains in the exact positions (14 and 15). Some of the kinetic energy of the electrons is transferred to the RE atoms in the depletion region and excitation occurs. The outcome can be classified as either radiative, with the energy emitted in the form of photons, and nonradiative, with the energy lost in the form of multiphonon emissions, Auger processes, or recombination at non-radiative defects (19 :6-7). The radiative and nonradiative losses can excite other atoms, both host material and impurity before emission from the sample occurs, but electrons taking part in such processes are undetectable and call for indirect detection methods to be used. The important phenomenon is the radiative transition that emits photons which then escape into the local environment where they can be detected and utilized. Depending on the excitation and de-excitation processes characteristic of the host lattice and impurity, the detected signal may be nonexistent or very weak to very strong. One would, of course, like to have a junction that emits strongly when minimal voltage is applied, but as is more often the case, a weak signal is detected under a moderate strength voltage, on the order of a volt. With these types of devices, increased voltage usually means more transferred electron kinetic energy and, thus, a resulting stronger detected signal. The excitation can only be seen when enough voltage is applied so that the energy bands shift closer together and the electrons become able to traverse the depletion region, recombine, and excite luminescence.

Following this rudimentary look at PL and EL, the method of luminescence detection and the equipment used is presented in the next chapter.

III. Experimental Procedure

Sample Preparation

The unimplanted pn/np-GaAs and pn-$Al_xGa_{1-x}As$ ($x=0.1, 0.3$) wafers were grown at Epitronics Corporation using the LEC/VGF process. Once received, they were diced into ¼" × ¼" square samples. All samples were then sent to Universal Energy Systems for Er and Nd implantation. Two different doses were desired (1×10^{13} and 5×10^{13} cm^{-2}), and so a total of four different implantations were performed (see Table 1 for implant energies and depths). Once the implantation was finished, the samples were annealed using the RTA process. The samples were rapid thermal annealed for 15 seconds at 750 °C based on Elsaesser's work (11). After making an identifying scribe mark on the back of each sample, half of the samples were set aside for immediate PL measurements. The other half were processed for EL using mesa diode lithography.

Mesa diode lithography is a multistep process yielding quality diode packages. The first step is to perform mesa photolithography which places a photoresist mask on the top of the material. After this has occurred, the mesas are photoetched before a second mask is put in place, which is needed for the ohmic contacts. The ohmic contacts are then produced and the second mask is photoetched. The need for the second mask is to prevent metallic "hairs" from being formed around the circumference of the mesa during the ohmic contact placement, which have the potential of shorting the diode. The second ohmic contact which forms the base contact is then deposited. An alloy anneal for deposited metalization is performed before the sample is diced into smaller pieces. Each piece is diced so as to contain about eight working diodes. The pieces are placed in a diode package which is more convenient form to work with and provides a strong protective backing to help prevent the semiconductor from breaking. This process yields about four diode packages from one ¼" × ¼" piece. The best diode package is used for the measurements, and the rest provide backup samples in case the primary sample becomes shorted or open and, therefore, unusable.

The final product of the lithographic process is a set of pn- and np-diode packages. A typical pn-diode package is shown in Figure 6. The wire contacts from the package casing to the mesa are made of a gold-zinc alloy for the contact to the p-type side and a nickel-germanium-gold alloy for the contact to the n-type material.

After each diode package was received, its voltage vs. current characteristics , or I-V curve, was checked on a Tektronix model 577 Curve Tracer. Because the diodes were to be connected in parallel, each diode in the package was checked to make sure it was not shorted or open, and also to determine if it was a leaky diode. This study was mainly concerned with forward biased diodes so the reverse bias characteristics of the diodes will not be given here, however, the reverse bias characteristics were investigated on the I-V curve to ensure that they were in fact diodes. A typical I-V curve is shown in Figure 7 for some of the diodes seen in this work.

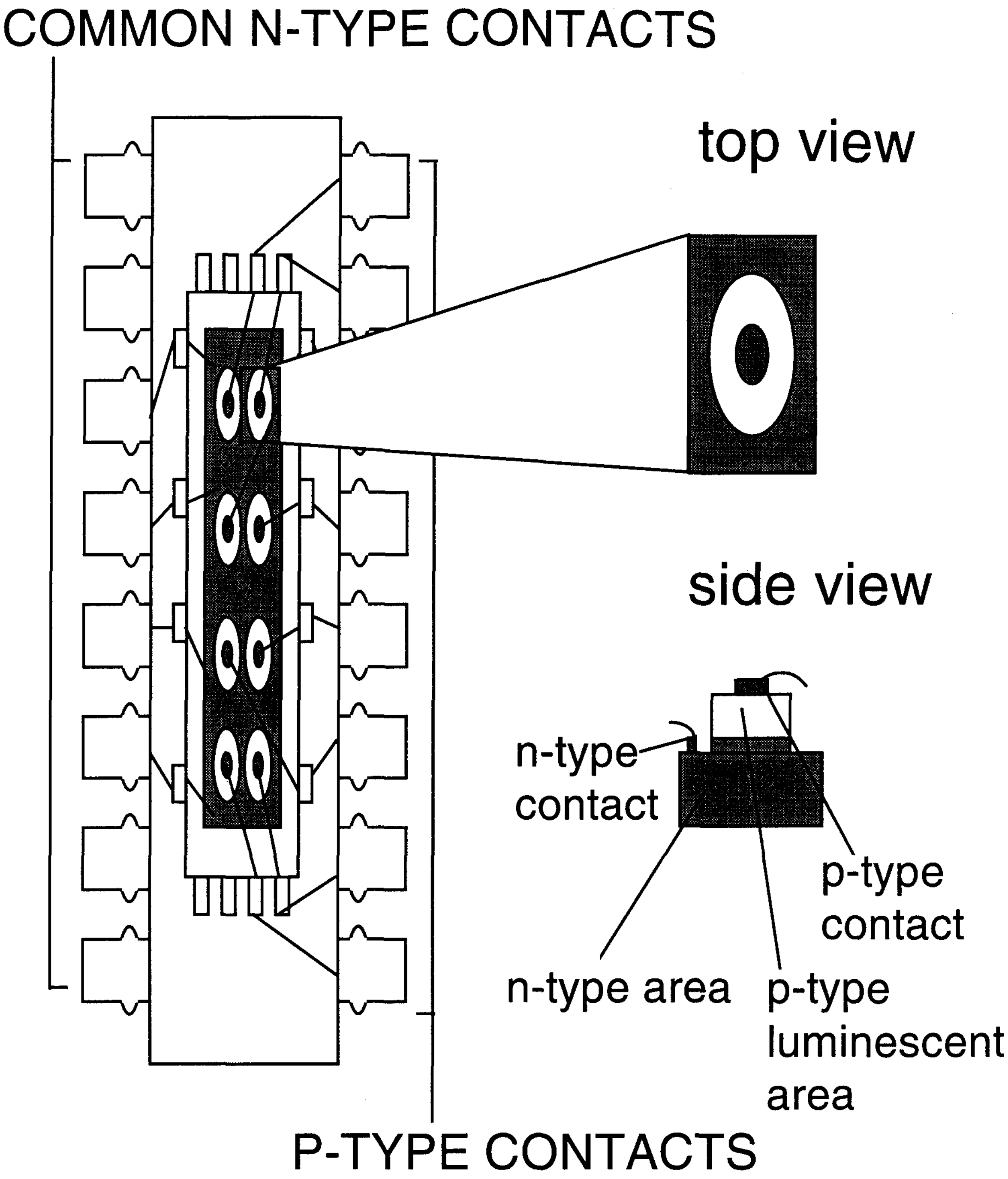

Figure 6. A package of mesa diodes used in electroluminescence measurements.

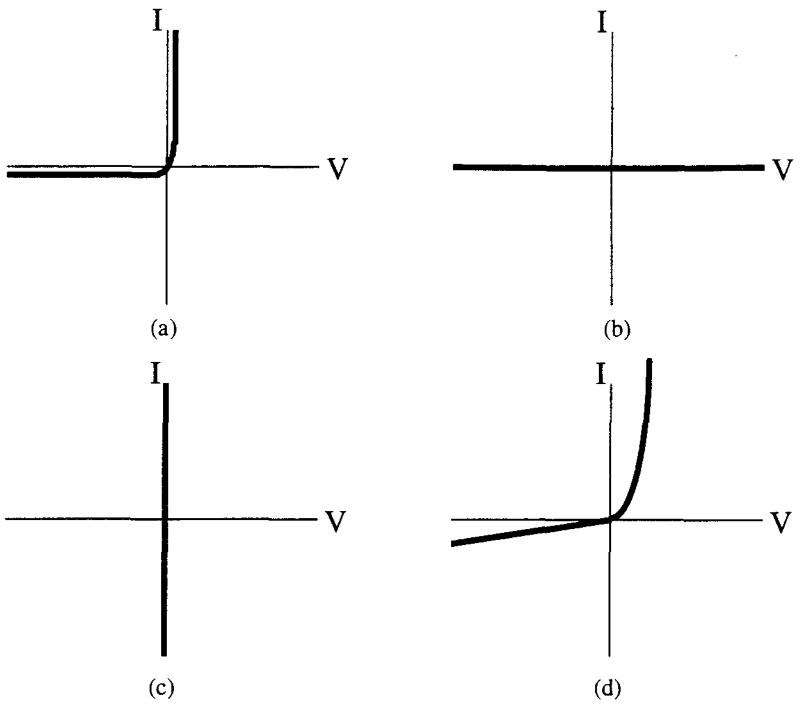

Figure 7. I-V curves of (a) a properly working diode, (b) an open diode, (c) a shorted diode, and (d) a leaky diode.

Equipment Setup

Once the diodes were checked for integrity, the good diodes were connected in parallel, mounted on beryllium oxide to prevent electrical shorting to the cold finger on which it was mounted, and inserted into a Janis Model 10DT Supervaritemp Optical Cryostat. The samples were then cooled to four degrees Kelvin with liquid helium that had a vacuum being applied to it so as to reach an operating temperature of ~2 K at which point the liquid helium becomes quiescent. As a result the sample chamber was maintained at about ~20 mTorr. Since the photon collection method for both PL and EL is the same, we shall first describe the sample excitation for each method before describing the collection of data.

For PL, the 5145 Å line from a Spectraphysics, model 2085A-20, argon ion laser was used to excite the sample. Care must be taken to tilt the sample so that the reflected laser beam does not go directly into the monochromator. The orientation of the sample surface was about ~92° to the incoming beam in the direction of the monochromator entrance slit. This prevented the beam from entering the slit and it also gave the highest luminescent signal. To attenuate unwanted plasma lines from the laser and prevent these lines from showing themselves in the data, a 514 nm ± 10 nm bandpass filter was placed before the laser entrance port of the cryostat and a 100 nm longpass filter was also used in front of the monochromator entrance slit. Before the beam entered the sample chamber, it was modulated with a chopper connected to a Stanford Research Systems model SR540 Chopper Controller to provide the detector with a sampled input. A diagram of the PL experimental apparatus is depicted in Figure 8.

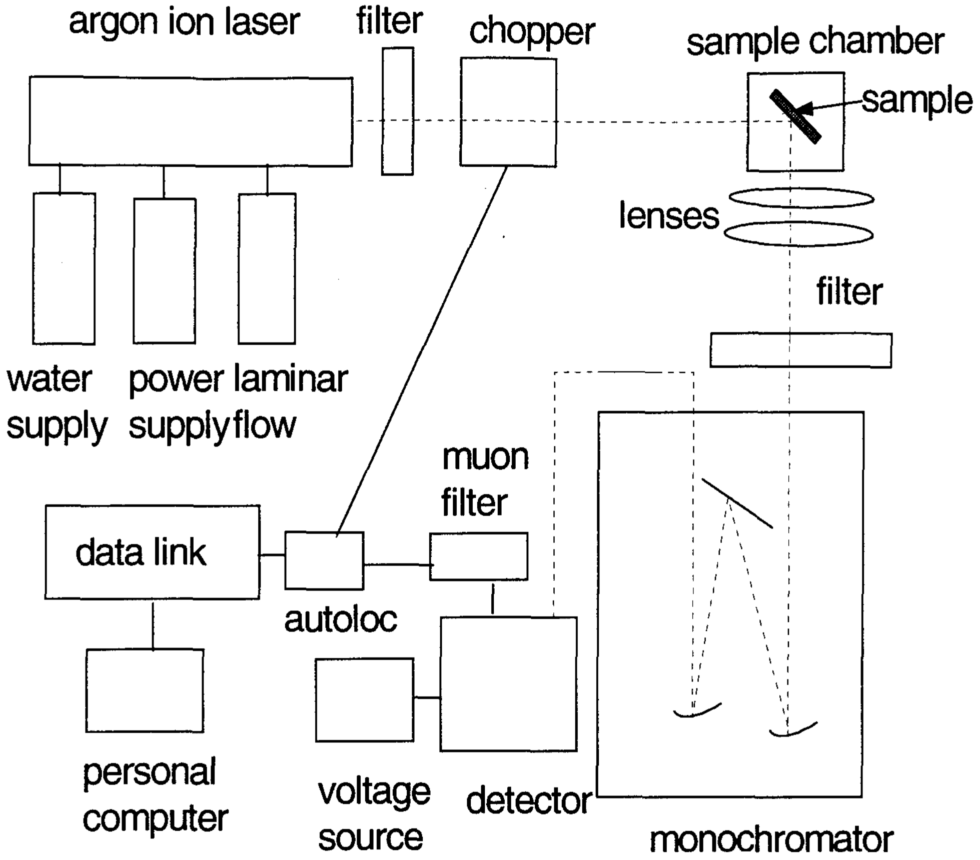

Figure 8. Experimental setup for photoluminescence.

For EL, after the diode package was inserted into the cryostat sample chamber, it was oriented with its surface directly towards the monochromator entrance slit. A voltage was applied with a Keithley model 238 High Current Source Measurement Unit until a signal was detected with a handheld FJW Optical Systems, Find-R-Scope® infrared viewer. The current source was routed through a Keithley model 8006 Component Test Fixture which converts a three lug triax input to a two lug coax output to the package. In the EL case, the chopper was placed in front of the entrance slit. This setup is shown in Figure 9.

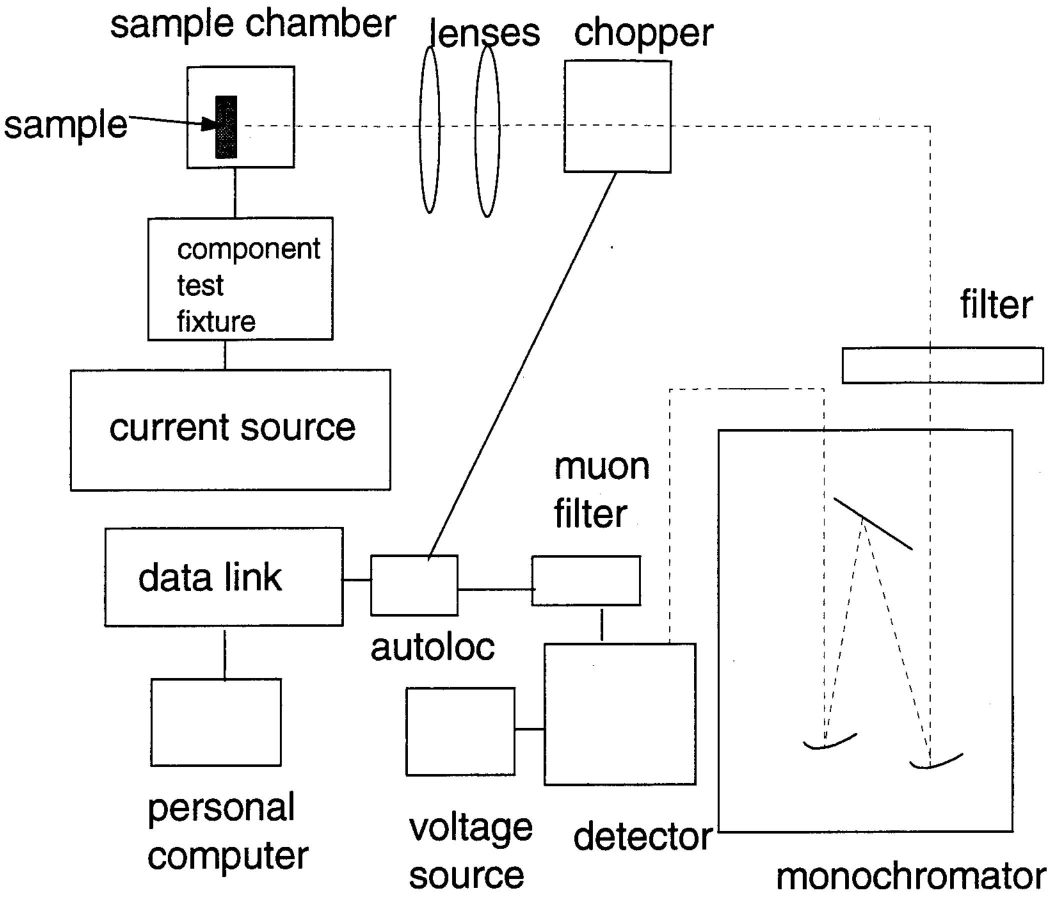

Figure 9. Experimental setup for electroluminescence.

Collection of emitted photons is the same for both EL and PL. So, once the luminescence is emitted from the sample it enters the Spex 750 Monochromator (600 grooves per millimeter, 1.25 μm blaze angle) and is absorbed by the Applied Detector Corporation's Model 403 I-R liquid nitrogen-cooled germanium detector which is connected to the NorthCoast Model 829B Muon Filter and the NorthCoast Model 823A Bias Supply. A responsivity curve for the germanium detector can be found in Figure 10 (20). The signal is then fed through the chopper controller into the Lock-In Amplifier and finally routed through the DM3000 monochromator controller where the measured results can be plotted vs. wavelength.

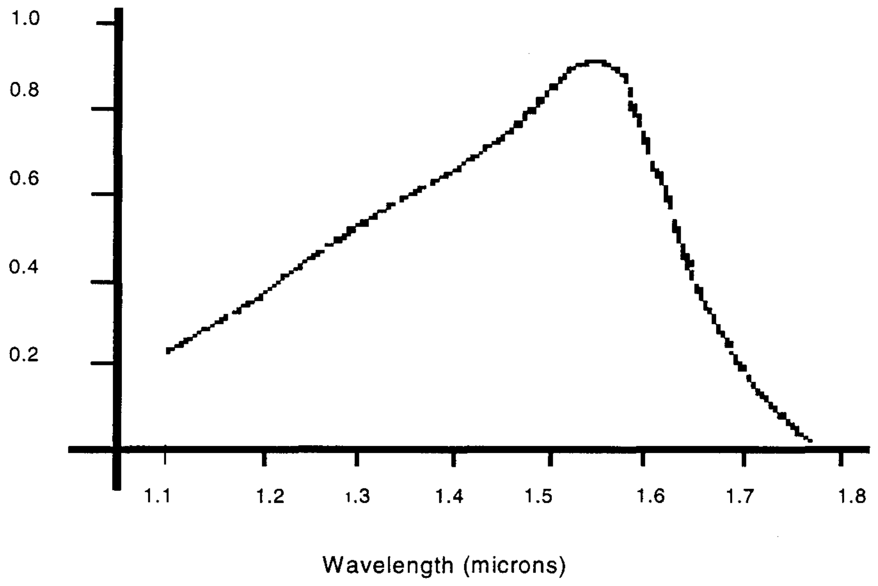

Figure 10. Responsivity curve for the NorthCoast Germanium IR detector. The vertical axis is in percent responsivity.

The signal itself can be maximized by adjustment of the sample orientation with respect to the entrance slit in conjunction with an adjustment in the position of the focusing lenses. This and the power applied to the sample, either laser excitation or applied voltage, affects signal strength. For EL, an initial signal is obtained by applying a forward bias equal to the previously measured room temperature turn-on voltage from the I-V curve tracer and then increasing it in increments (usually to near 100 mA for the samples used in this study).

Calibration

Once the equipment is arranged as stated in the previous section, the next step is to calibrate the detector with a known source. The simplest method of calibrating the detector is by using the second order peak (12656 Å) from a low power HeNe laser. This peak is close to the Er^{3+} (14000-17000 Å) and Nd^{3+} (15000-12000 Å) regions of interest, so confidence that the detector/grating response is not skewed in one direction or another can be attained. This method is used for daily calibrations to provide a quick check to make sure the monochromator-detector wavelength axis is the same as the day before. The laser is sent through the chopper and into a fiber optic cable which effectively diffuses the beam. The diffuse light passes through the last of the focusing lenses and into the monochromator entrance slit. Even though it is diffuse, the laser is of sufficient intensity to damage the detector so either a filter has to be placed in the beam or the slit width of the monochromator is decreased. Because high resolution of the spectra was desired, the slits were closed down to between 10 and 30 microns anyway, thereby decreasing the incident intensity and increasing the spectral resolution in one step. The resulting 12656 Å peak can be scanned and its position on the wavelength axis will indicate if the detector is misaligned. Subtractions and additions to the wavelength axis are then performed to correct for this misalignment. This short calibration is performed every day before actual rare-earth measurements are taken. With this short wavelength-axis correction performed, a thorough calibration of the system response can be accomplished. In order to do this calibration, an Electroptical Industries, Inc. Model WS143 Blackbody Source operating at 1273 K connected to an Electroptical Industries, Inc. Model 215B Temperature Controller is placed in front of the entrance slit to verify the responsivity curve provided by the manufacturer of the detector. Since the detector counts photons, we need to know the photon spectral radiance. This can be calculated by

$$L(\lambda,T)=\frac{2c}{\lambda^4}\cdot\frac{1}{e^{(\frac{hc}{\lambda kT})}-1}, \qquad (1)$$

where h is Planck's constant, k is Boltzmann's constant, c is the speed of light, T is temperature of the blackbody in degrees Kelvin, and λ is the wavelength (21 :49). The measured blackbody data, which is affected by the combination of the detector response and monochromator grating, can then be compared to the calculated curve to determined the efficiency of the detector as a function of wavelength. This work is primarily concerned with the wavelength range of 10500 Å to 17000 Å, where the loss in efficiency in the RE peaks is minimal. If we were interested in wavelengths near the drop-off points of the detector efficiency we could obtain a correction factor based on the difference in the two blackbody curves. The measured and calculated blackbody curves are presented in Figure 11.

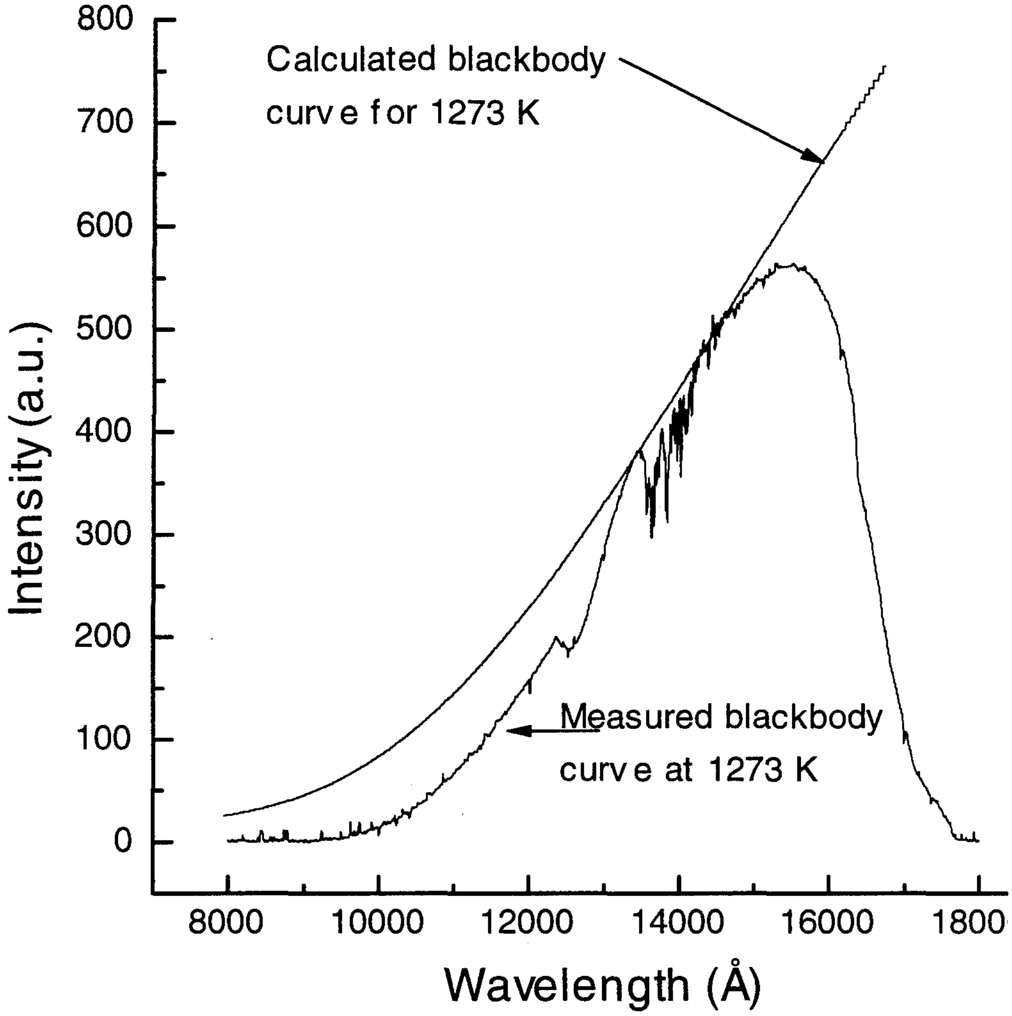

Figure 11. A comparison of the measured to calculated photon spectral radiance for a 1273 K blackbody source for the detector and grating equipment combination.

When this system calibration has been completed, we know what spectral data corrections must be implemented. With this in mind, we now turn to the results of this work.

IV. Results and Discussion

The main thrust of this work is the comparison of observed PL data with observed EL data. First, the PL measurement results of the MOCVD-grown Si:Er will be presented, followed by results of the PL measurements of the RE^{3+} implanted samples, and finally, the results of the EL measurements

Photoluminescence of MOCVD-Grown Er-doped Si Samples

The MOCVD-grown samples supplied by University of Vermont were initially grown as part of a fractional factorial study, where a set of variables is defined and assigned either a HI or a LO value in a given sample. The parameters varied were (A) metalorganic source temperature -- a LO level being 130 °F, a HI level being 140 °F, (B) silane (SiH_4) flow -- LO: 2.5 sccm and HI: 5.0 sccm, (C) hydrogen presence during growth -- LO: no and HI: yes, and (D) growth time -- LO: 35 minutes and HI: 70 minutes. Figure 12 shows the PL results for samples 68-78. The sample reference notation is as follows: an **a**, **b**, **c**, or **d** after the sample number indicates that particular parameter was held HI and an **L** indicates all parameters were held LO for that sample.

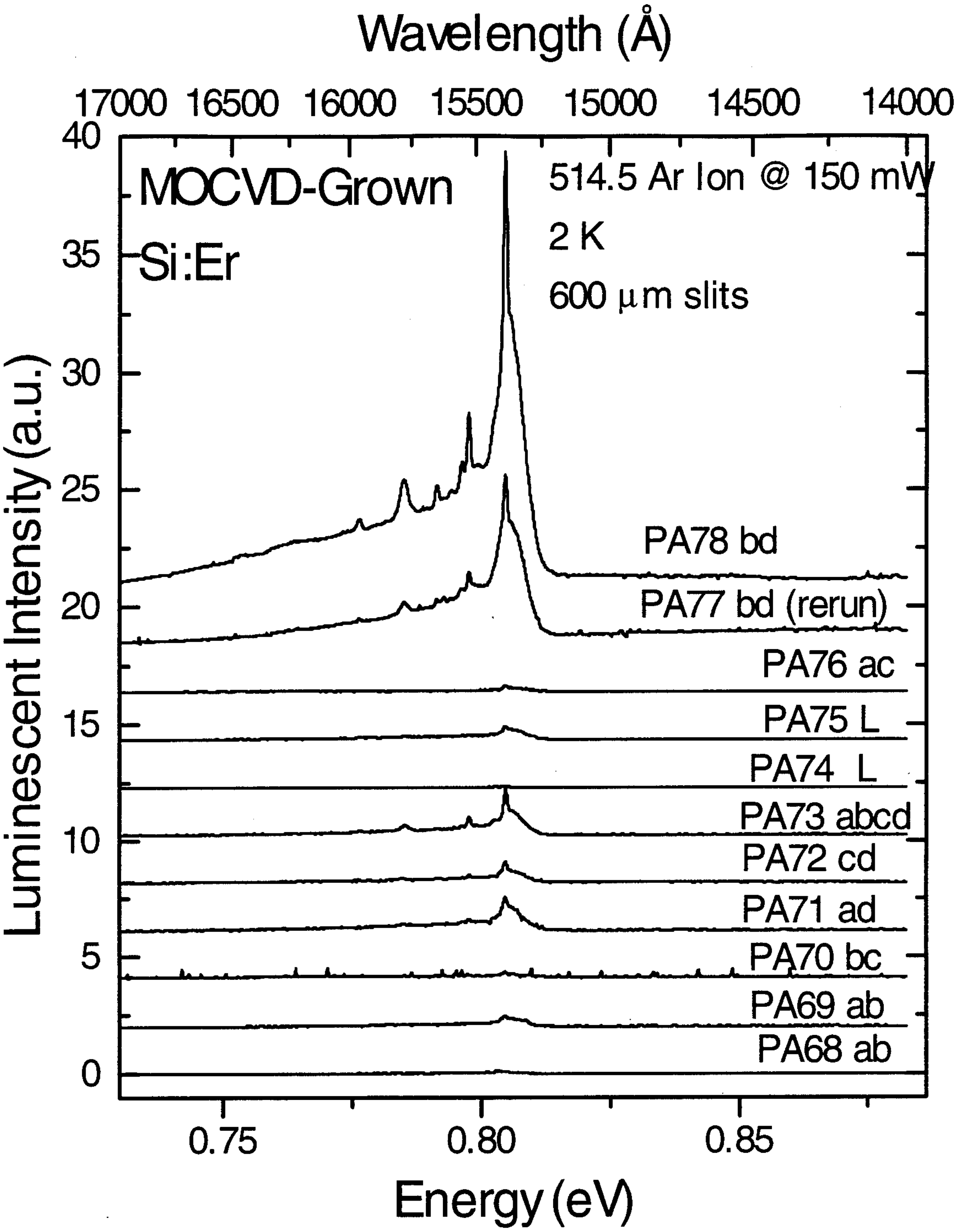

Figure 12. Photoluminescence measurements of MOCVD-grown Si:Er.

From Figure 12, one can see that samples PA78, PA77, PA73, PA72, and PA71 have the highest intensities of the entire group with a descending order. These samples were fabricated using the HI setting of growth time (70 min) which appears to be the dominant variable in this growth process. Another subset of samples from the group were those grown with a 5.0 sccm silane flow rate. From Figure 12, one can see that most of the samples grown with the HI silane setting (PA78, PA77, PA73, and PA69) display luminescence but the luminescent intensity is not as strong as from those samples grown at the HI setting for growth time. Actually, it again appears that the growth time of the sample is the most dominant factor in the process. All of the samples grown at the HI setting of 70 minutes produce at least a noticeable signal, while an increased silane flow rate, which appears to be the second most important factor in the process, only mildly enhances the Er^{3+} emissions when grown at the LO setting of 35 minutes. The strongest intensity sample, PA78, was grown under both of these conditions. It's possible that the longer growth time increased the Er^{3+} dose while the increased silane flow rate prevented the Er^{3+} ions from occupying substitutional sites resulting in a higher concentration of interstitial ions and higher intensity PL. In order to verify this proposed process, a sample with a HI growth time and all other factors LO would be needed. Unfortunately, a sample with these characteristics was unavailable.

Host Excitation Results

In order to adequately compare signals produced from the RE implanted samples, a knowledge of the PL spectra of the host material is required. Figure 13 shows the background signal obtained from illuminating the target sample with 47 mW from an Ar ion 5145 Å laser line.

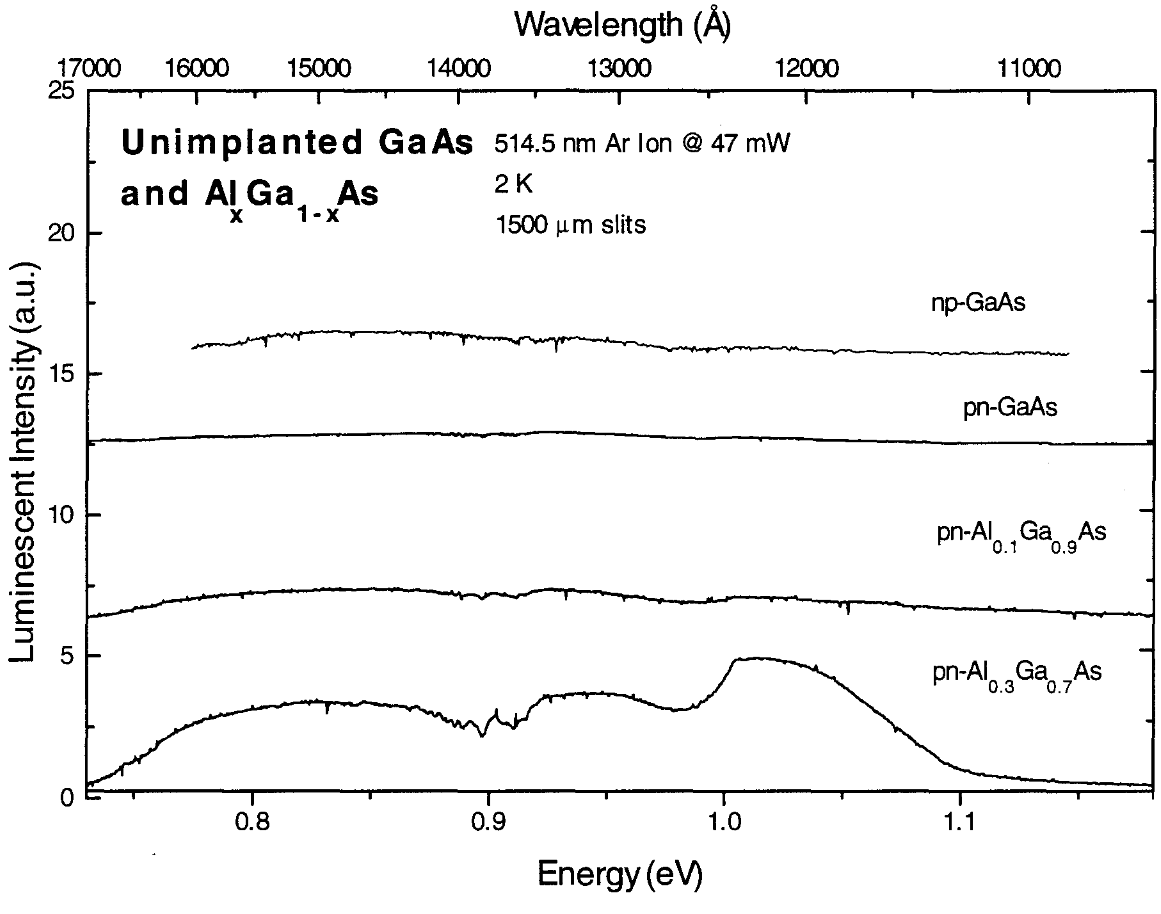

Figure 13. Photoluminescence spectra obtained from illuminating unimplanted np- and pn-GaAs and pn-$Al_xGa_{1-x}As$ with 47 mW from an Ar ion 5145 Å line.

From Figure 13, we see that there is a sufficiently high intensity from the host $Al_xGa_{1-x}As$ itself to be a potential problem, i.e. if the host material itself produces too much background luminescent intensity it may drown out the RE signal. There is some signal from the GaAs samples but comparatively much less than the $Al_xGa_{1-x}As$. The origin of the sudden intensity decrease around 12400 Å is unknown but suspected to be related to the blaze of the monochromator grating.

Photoluminescence vs. Rare-Earth Ion Dose and Al Mole Fraction

Since we now have an idea what to expect from the host material itself, a comparison of the different doses of Er in np-GaAs, pn-GaAs, and pn-$Al_xGa_{1-x}As$ structures can be made. Figure 14 and Figure 15 show the relative luminescent intensities for different Er^{3+} doses in the np- and pn-GaAs. Relative luminescent intensities for Er^{3+} in np- and pn-AlGaAs is likewise shown in Figure 16 and Figure 17.

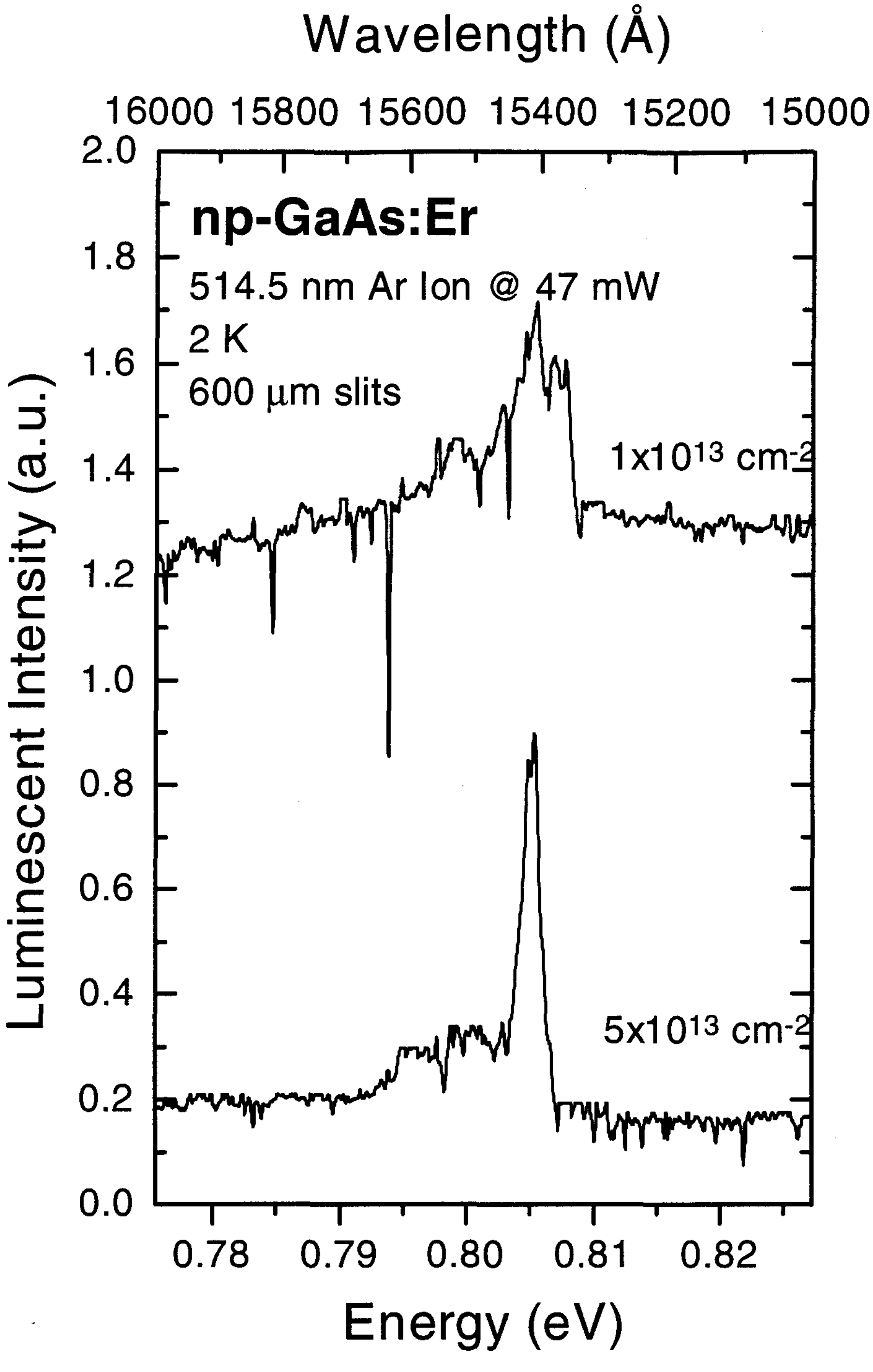

Figure 14. Photoluminescence spectra measured from Er implanted np-GaAs with doses of 1×10^{13} cm^{-2} and 5×10^{13} cm^{-2}.

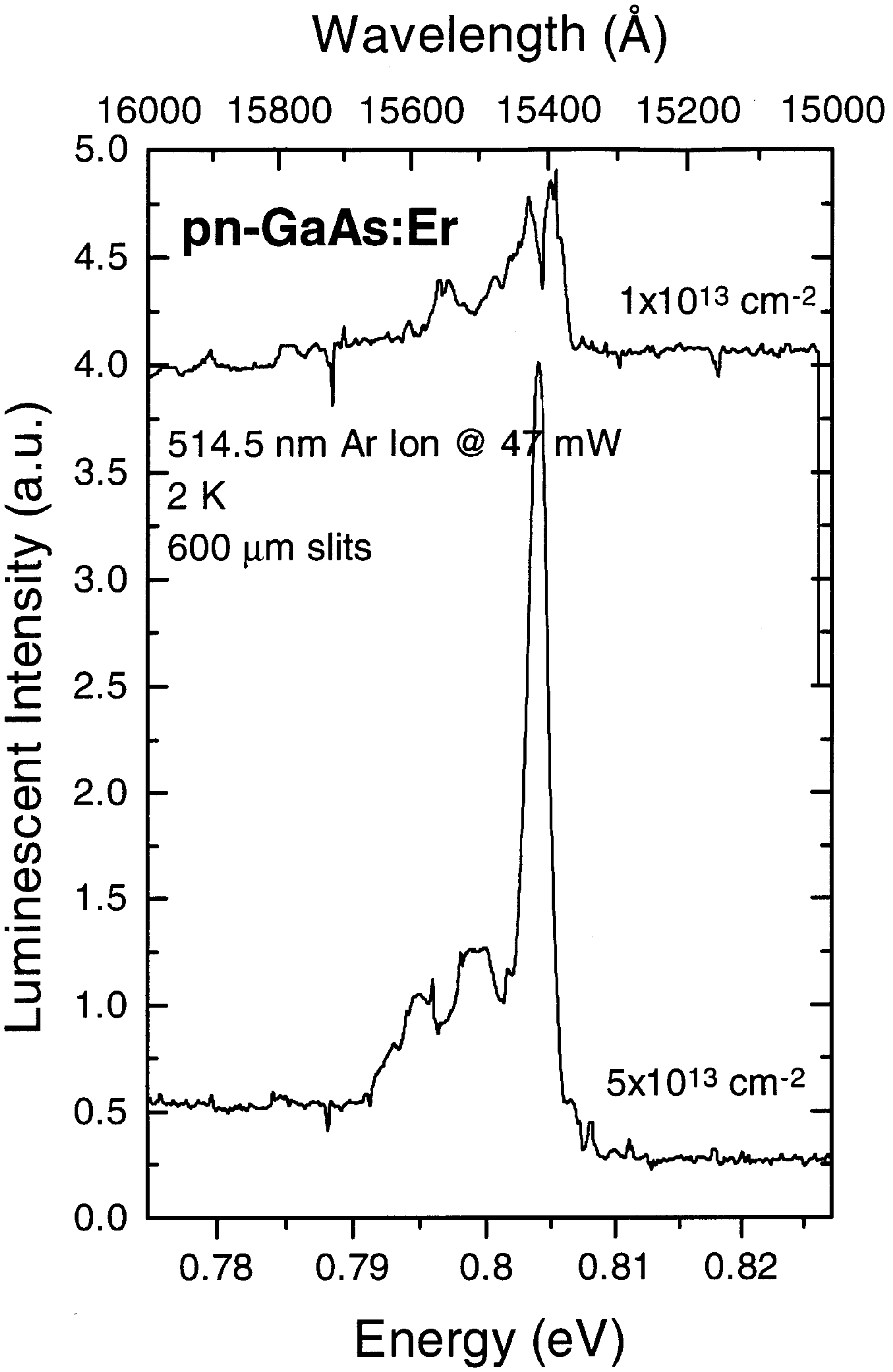

Figure 15. Photoluminescence spectra measured from Er implanted pn-GaAs with doses of 1×10^{13} cm^{-2} and 5×10^{13} cm^{-2}.

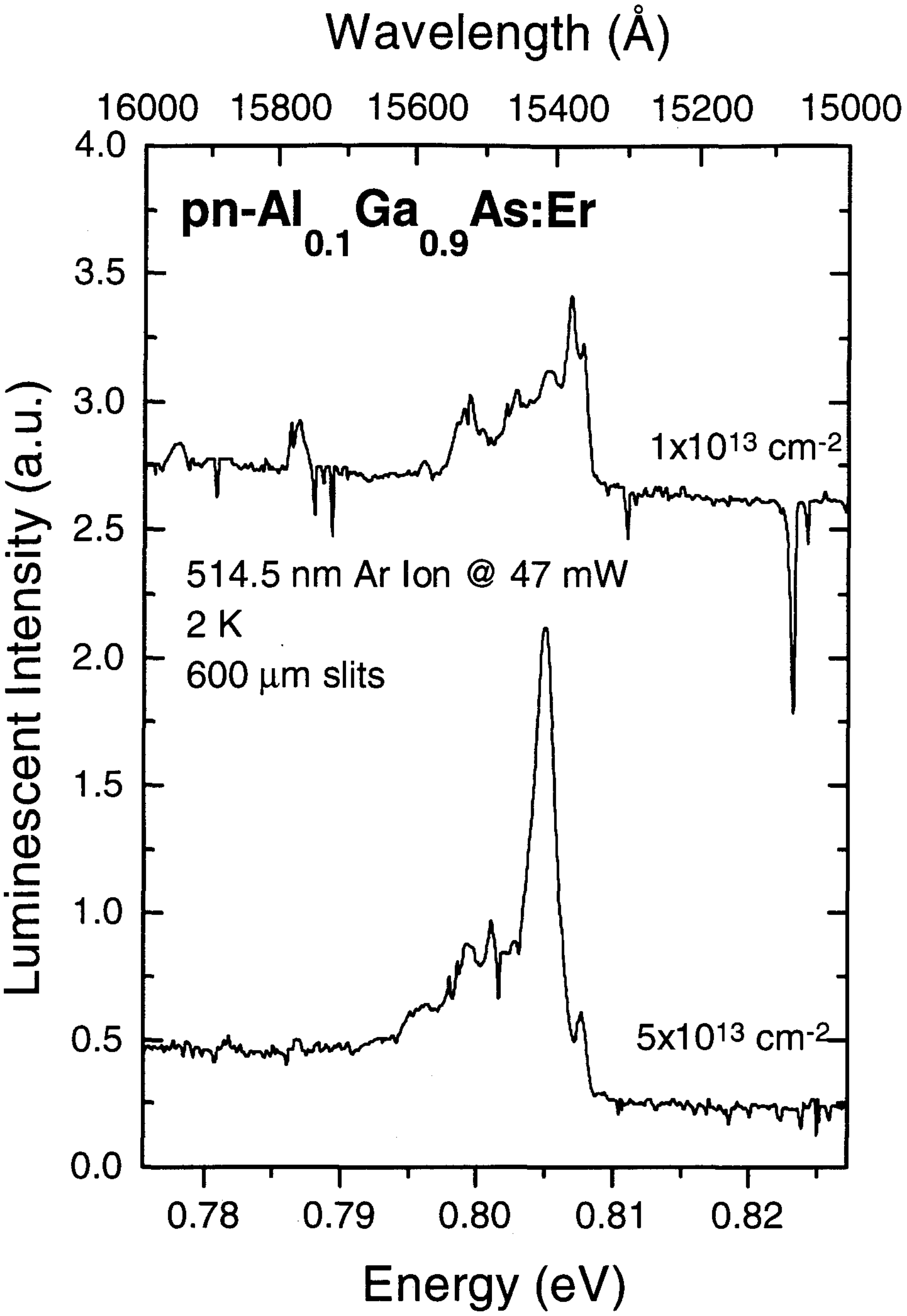

Figure 16. Photoluminescence measured from Er implanted pn-type $Al_{0.1}Ga_{0.9}As$ with doses of 1×10^{13} cm^{-2} and 5×10^{13} cm^{-2}.

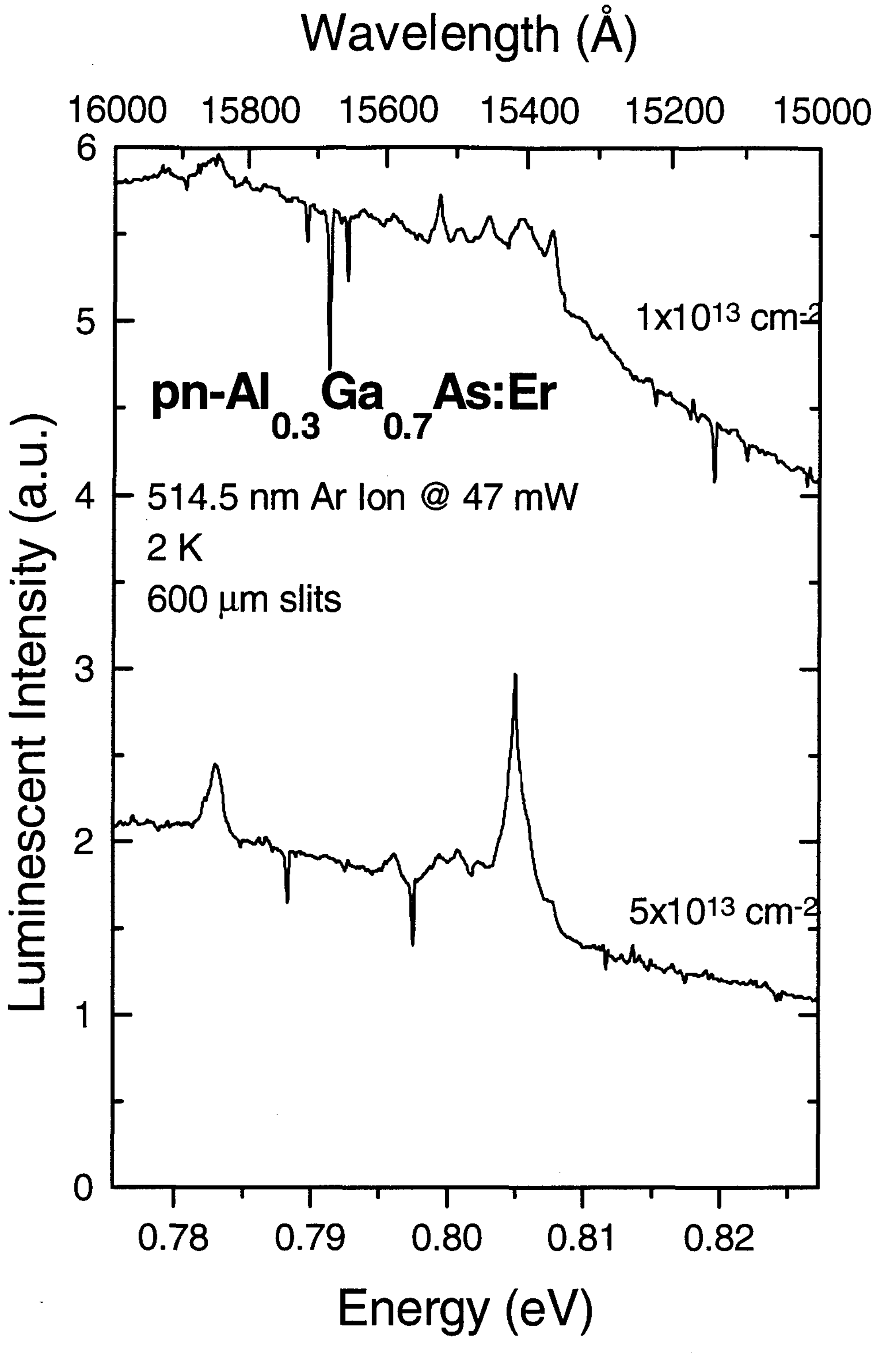

Figure 17. Photoluminescence measured from Er implanted pn-type $Al_{0.3}Ga_{0.7}As$ with doses of 1×10^{13} cm^{-2} and 5×10^{13} cm^{-2}.

In all cases for Er implanted GaAs and $Al_xGa_{1-x}As$, the 5×10^{13} cm^{-2} dose produced a stronger luminescent signal than the 1×10^{13} cm^{-2} dose. By increasing the Al mole fraction from 0.1 to 0.3, the background from the host lattice increases to the point where the erbium peaks are almost completely obscured by the lattice signal. Comparing the relative peak intensities of the 5×10^{13} cm^{-2} dose, as is shown in Figure 18, it appears that the strongest signal comes from the pn-GaAs. The second most intense signal comes from the pn-$Al_{0.1}Ga_{0.9}As$ and then from the pn-$Al_{0.3}Ga_{0.7}As$. These results hint that stronger luminescence is emitted from pn- materials rather than np- materials. Since the peak concentration of the RE ions are calculated to be in the n-type regions for the pn-junctions, we could hypothesize that the incoming photons transfer energy in a more direct path to the 4f-shell electrons than in the p-type material. Possibly, if the RE ions were in the p-type region, incoming photons would have to excite host lattice electrons into all the local holes before transferring energy to the RE 4f-shell.

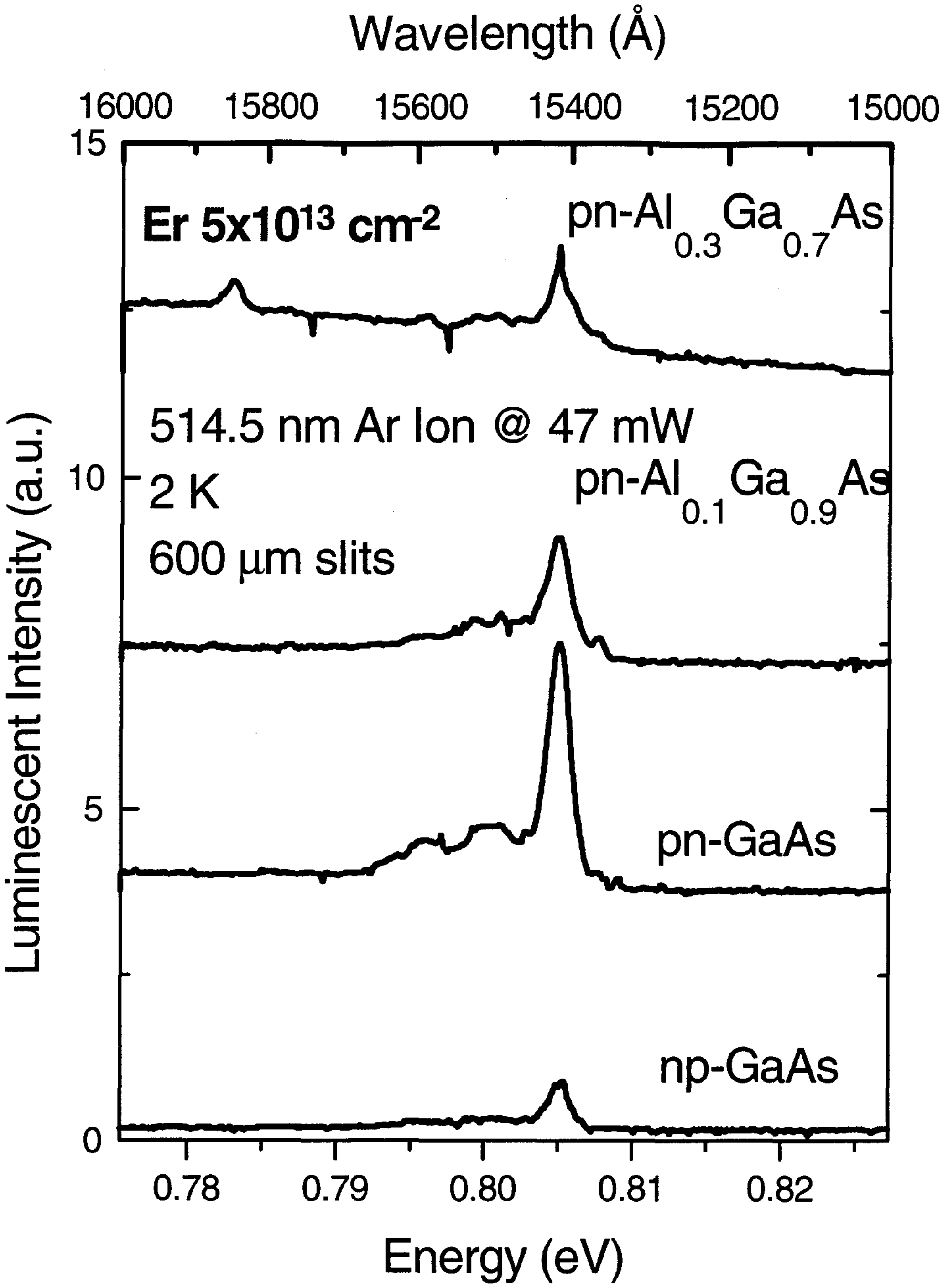

Figure 18. Photoluminescence measured from an Er dose of 5×10^{13} cm^{-2} in the np- and pn-GaAs and pn-Al$_x$Ga$_{1-x}$As.

Neodymium-implanted GaAs and $Al_xGa_{1-x}As$ show much of the same phenomenon. In Figures 19, 20, 21, and 22, we find that the luminescence from samples with a 1×10^{13} cm^{-2} dose is lower in intensity than that for their 5×10^{13} cm^{-2} counterparts. The effect of Al on the luminescent center is quite dramatic in Figure 21 and Figure 22, as the RE signal is very weak in the $Al_{0.1}Ga_{0.9}As$:Nd for a dose of 1×10^{13} cm^{-2}, not present at all in the $Al_{0.1}Ga_{0.9}As$:Nd for a dose of 5×10^{13} cm^{-2}, and is barely discernible in $Al_{0.3}Ga_{0.7}As$. Again, the host signal increases when the dose is increased from 1×10^{13} cm^{-2} to 5×10^{13} cm^{-2} but seems to remain the same when increasing the Al mole fraction from 0.1 to 0.3

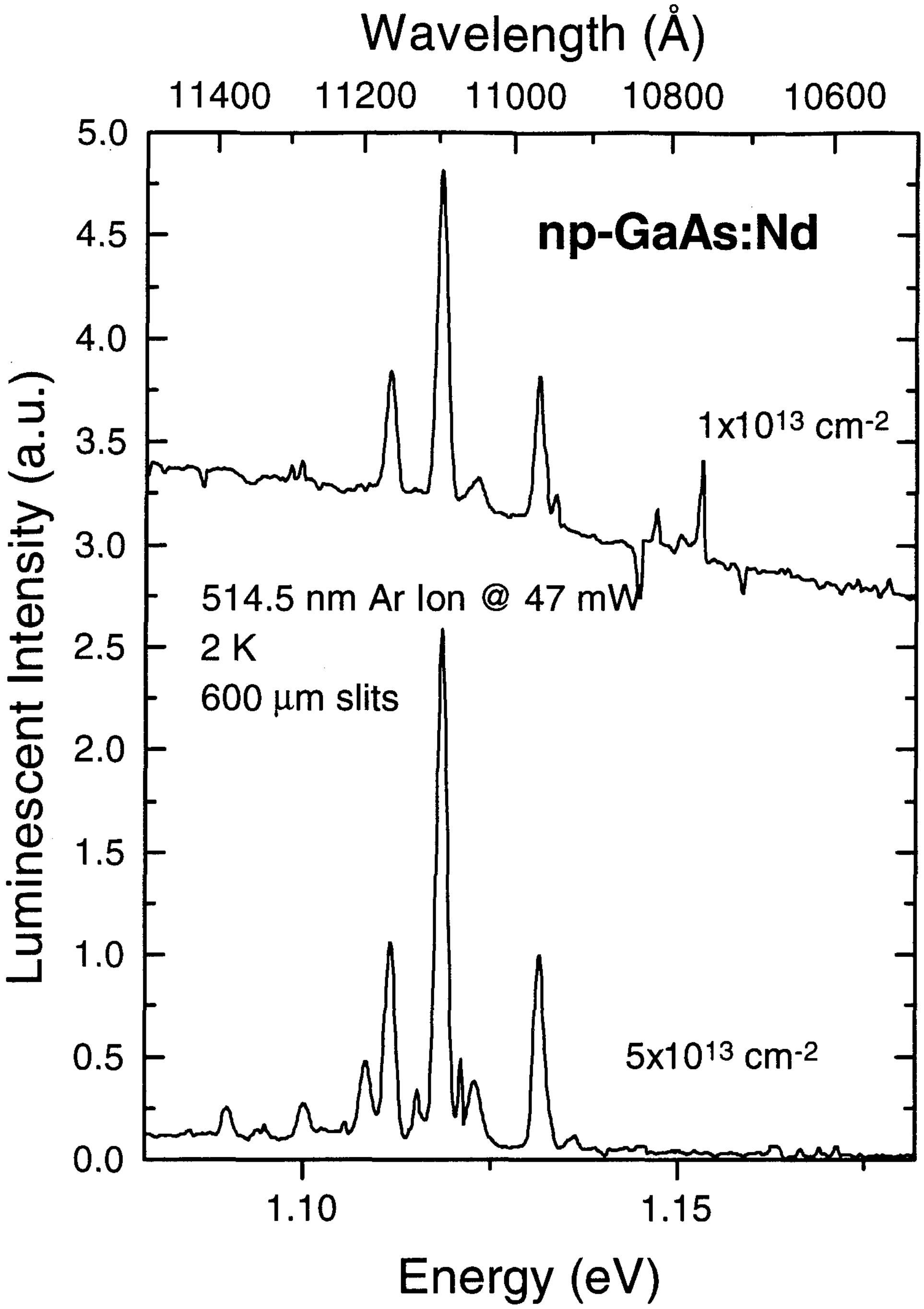

Figure 19. Photoluminescence measured from Nd implanted np-type GaAs with doses of 1×10^{13} cm^{-2} and 5×10^{13} cm^{-2}.

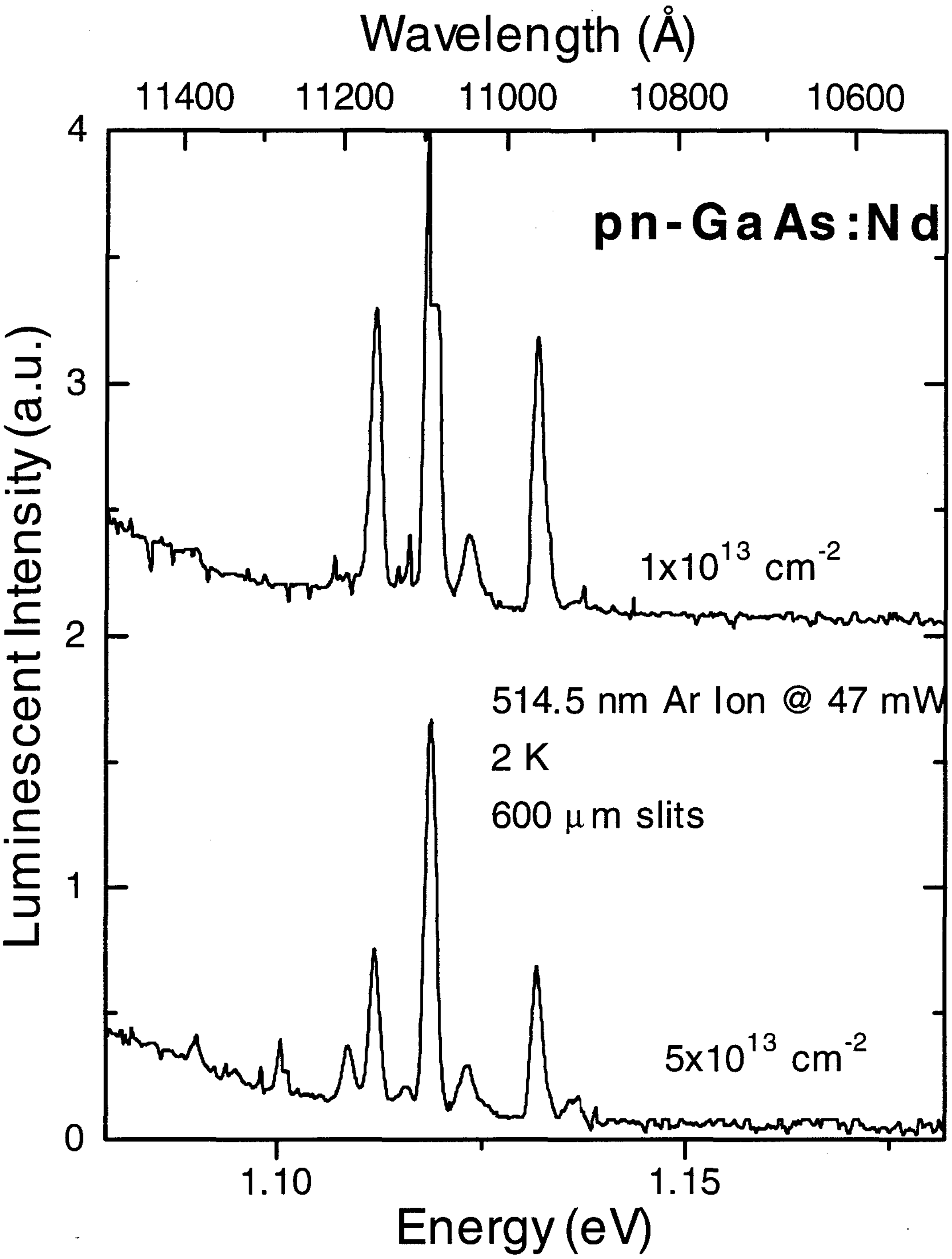

Figure 20. Photoluminescence measured from Nd implanted pn-type GaAs with doses of 1×10^{13} cm^{-2} and 5×10^{13} cm^{-2}.

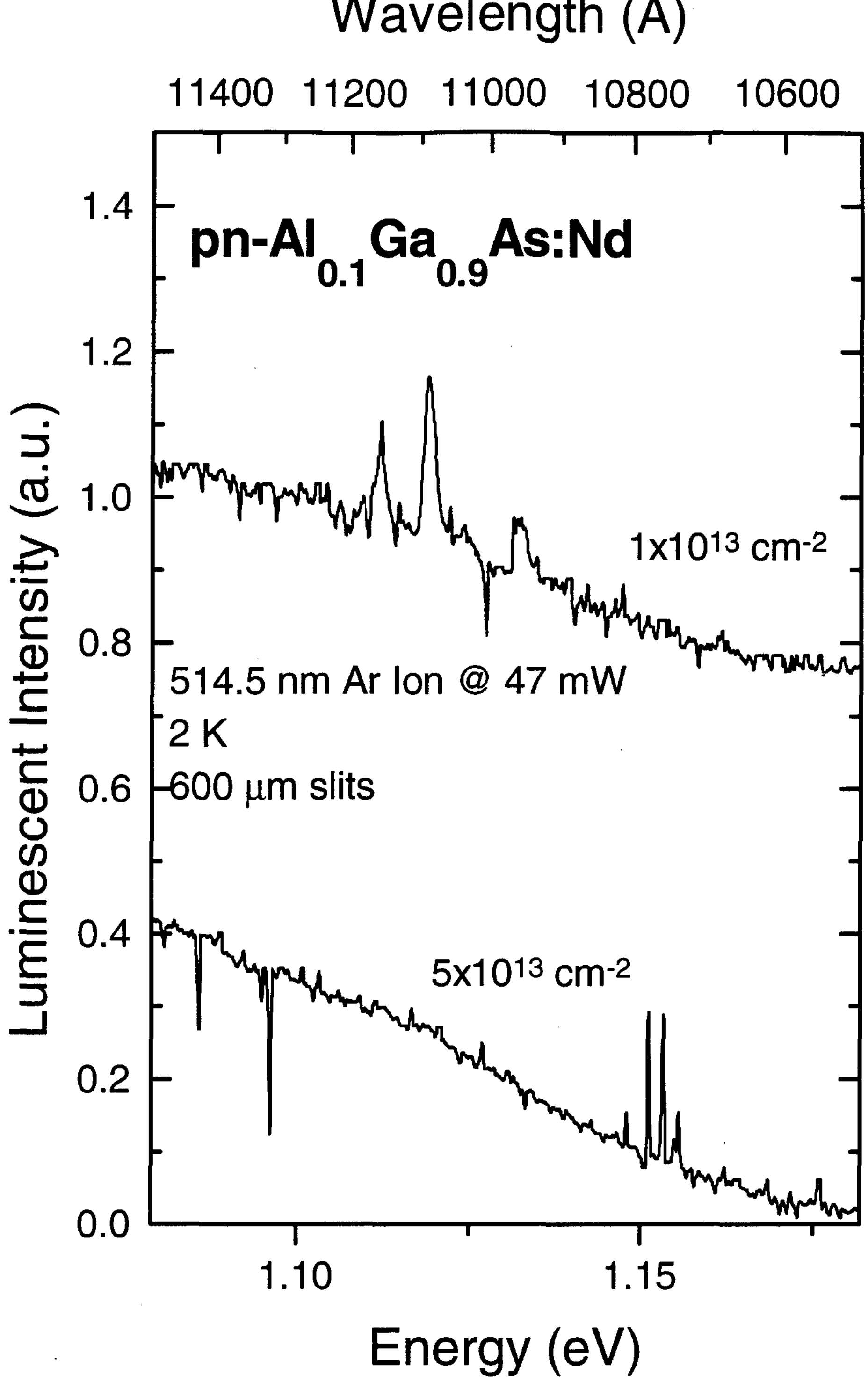

Figure 21. Photoluminescence measured from Nd implanted pn-type $Al_{0.1}Ga_{0.9}As$ with doses of 1×10^{13} cm^{-2} and 5×10^{13} cm^{-2}.

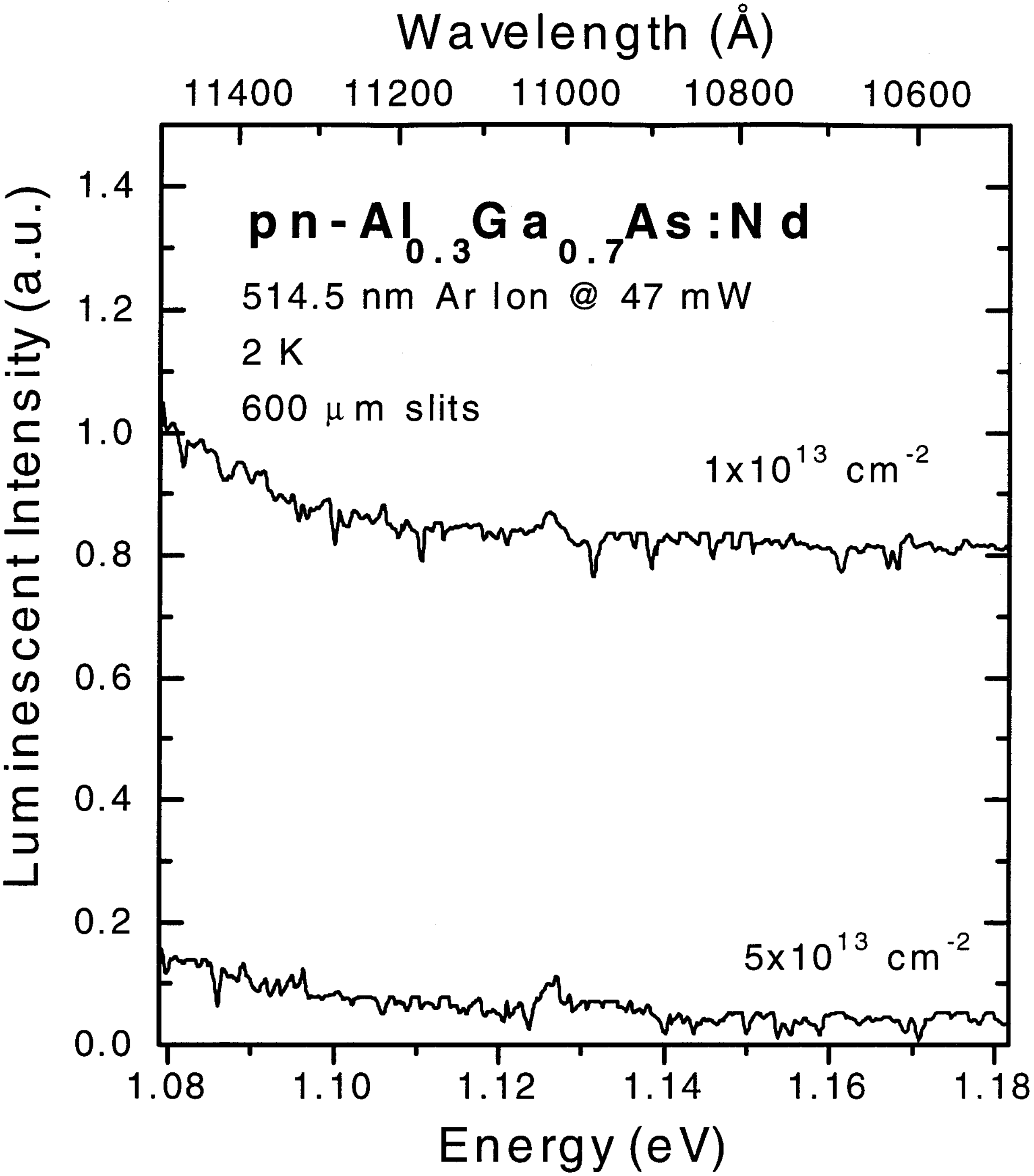

Figure 22. Photoluminescence measured from Nd implanted pn-type $Al_{0.3}Ga_{0.7}As$ with doses of 1×10^{13} cm^{-2} and 5×10^{13} cm^{-2}.

The RE dose that produced the strongest intensity signal was again 5×10^{13} cm^{-2}. The spectra obtained from all four materials implanted with Nd is shown in Figure 23. Here, we find slightly different results from the Er-implanted samples. Now the np-GaAs produces a stronger signal than the pn-GaAs. In the $Al_{0.1}Ga_{0.9}As$, there is a cluster of peaks that resemble those of Nd but which are grossly reduced in energy and much smaller in intensity compared to the GaAs samples. The most probable explanation is that they are noise.

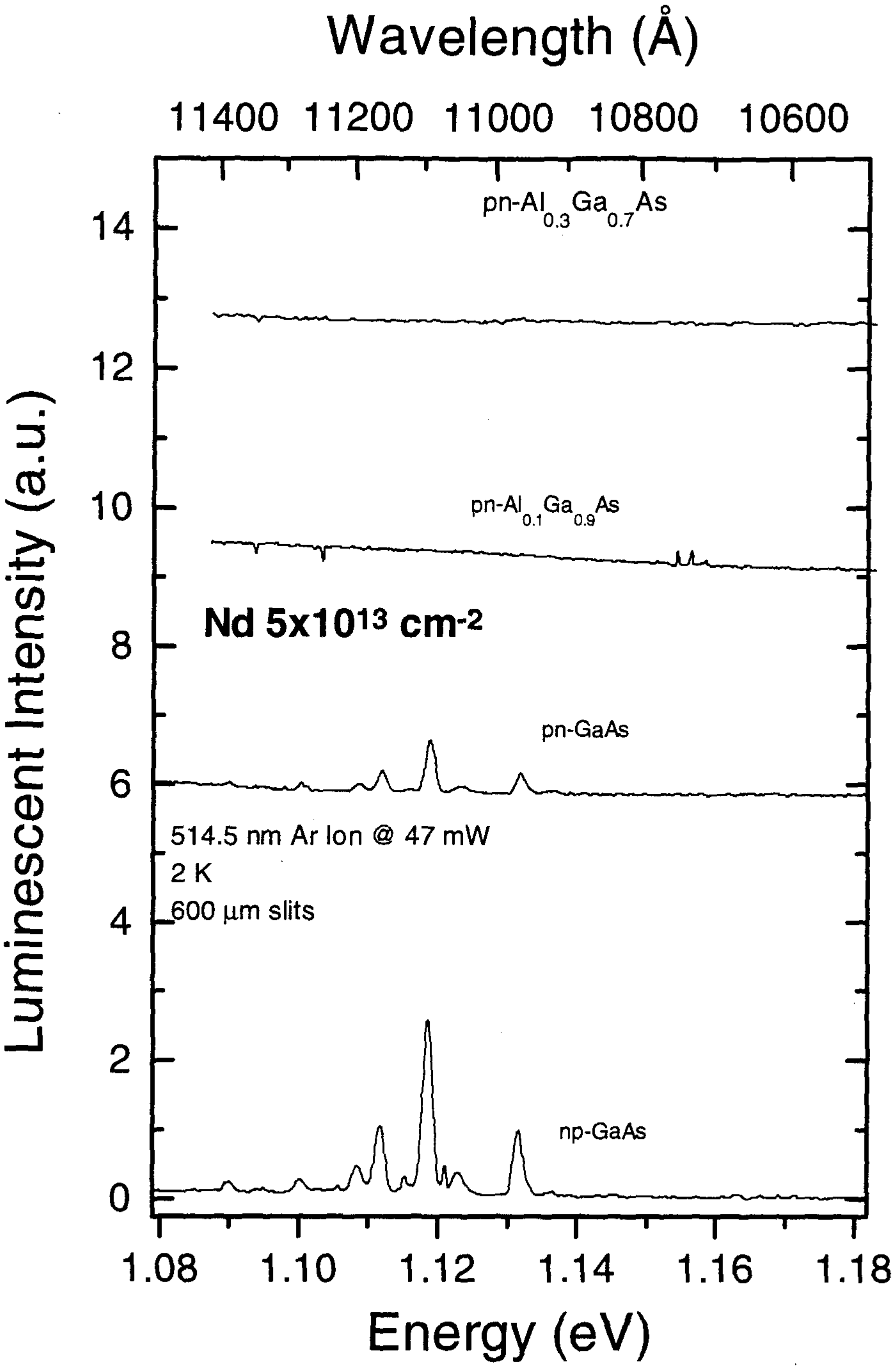

Figure 23. Photoluminescence results from the np- and pn-GaAs and pn-$Al_xGa_{1-x}As$ with a Nd dose of 5×10^{13} cm^{-2}.

Excitation Power vs. Luminescent Output

Significant energy barriers may be present in the lattice which must be overcome in order to excite the RE ions. In order to obtain a high intensity signal, it is necessary to find the optimum input laser power to get the most RE luminescence. The samples showing the strongest PL, pn-GaAs:Er, Nd 5×10^{13} cm^{-2} were selected and were subjected to input laser powers of 70 mW, 300 mW, 600 mW and 900 mW. The spectra of unimplanted pn-GaAs along with the RE-implanted pn-GaAs results are shown in Figures 24, 25, and 26.

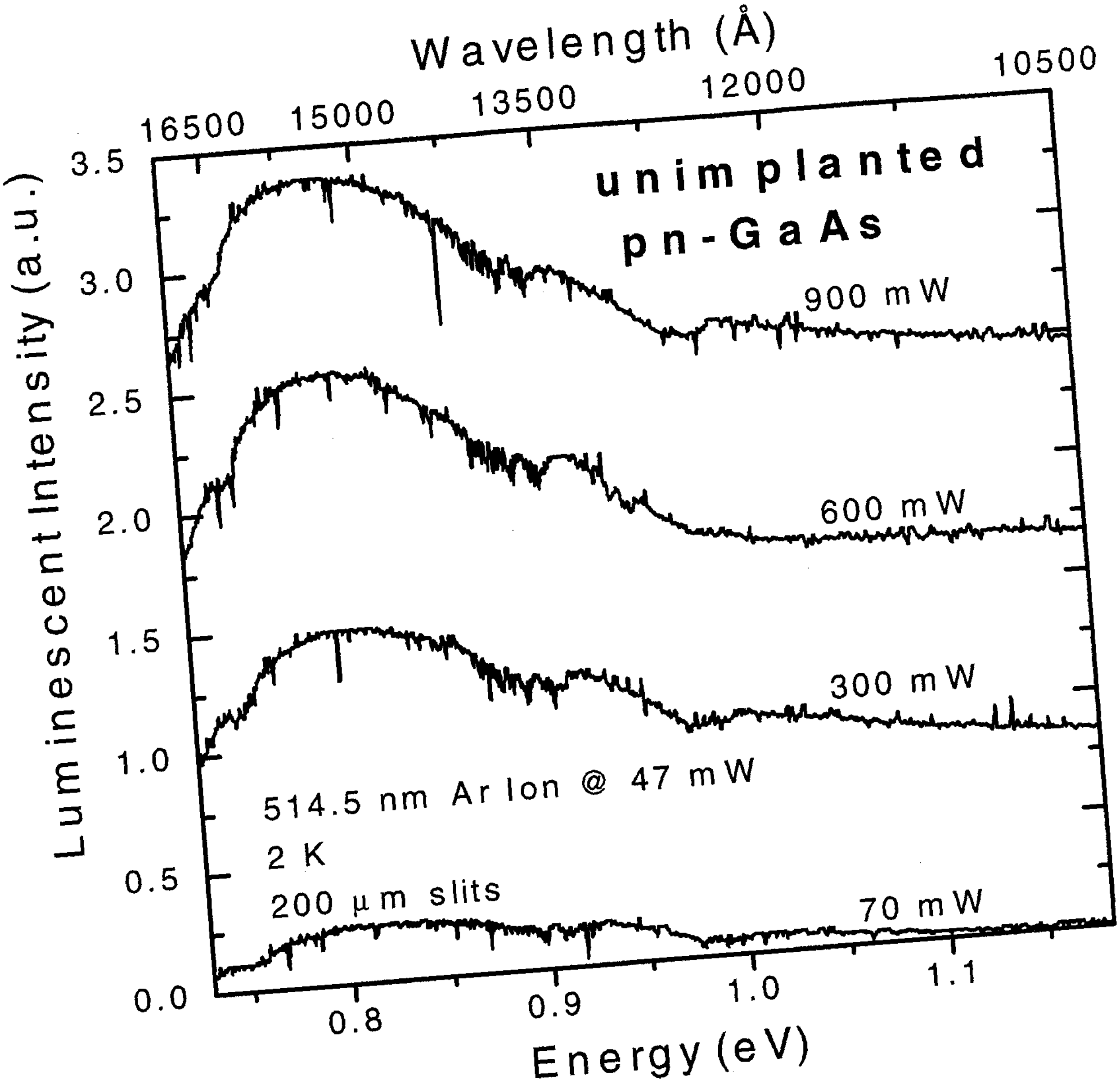

Figure 24. Photoluminescence measured from the unimplanted pn-GaAs as a function of laser excitation power.

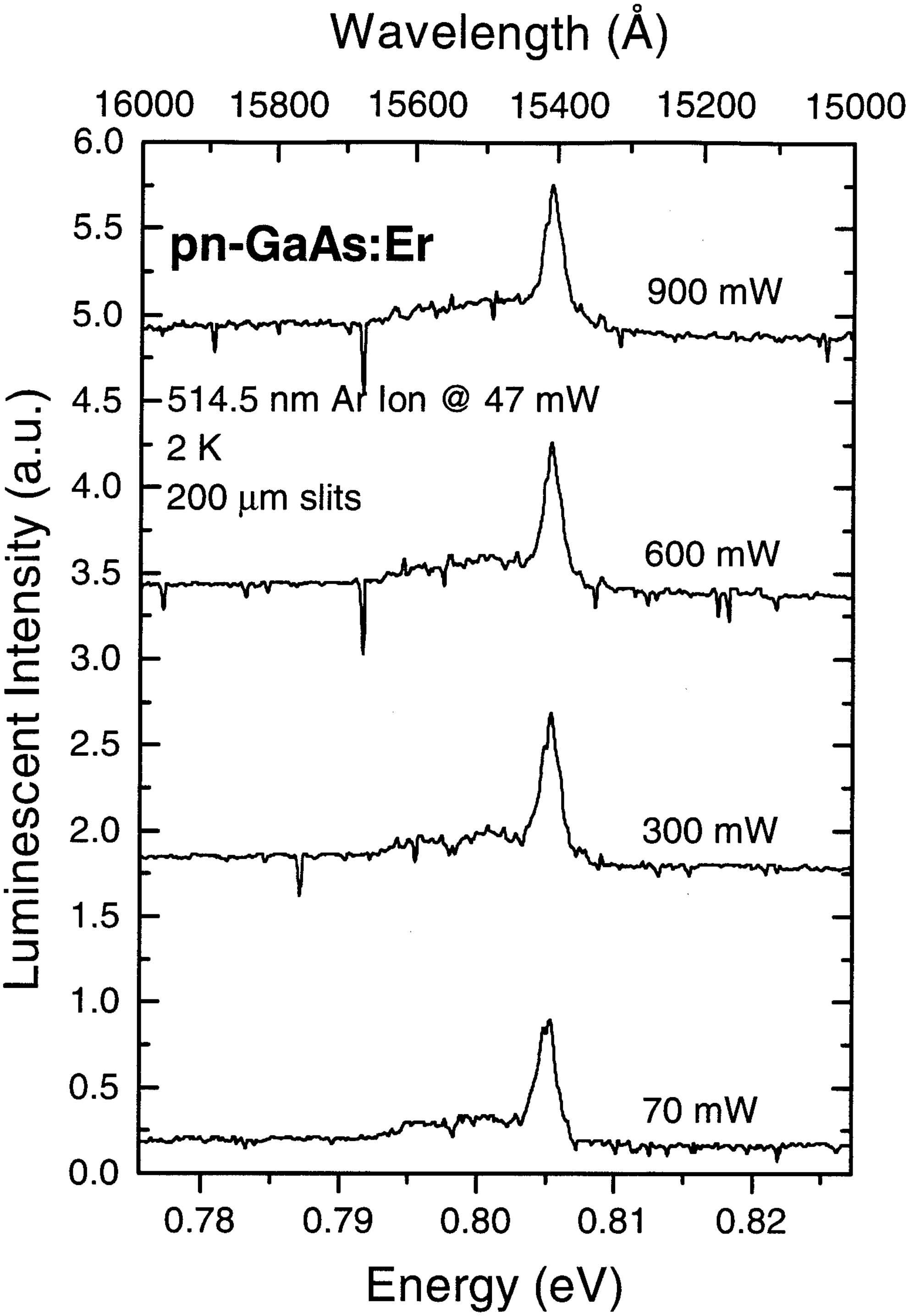

Figure 25. Photoluminescence measured from the pn-GaAs implanted with Er at a dose of 5×10^{13} cm^{-2}.

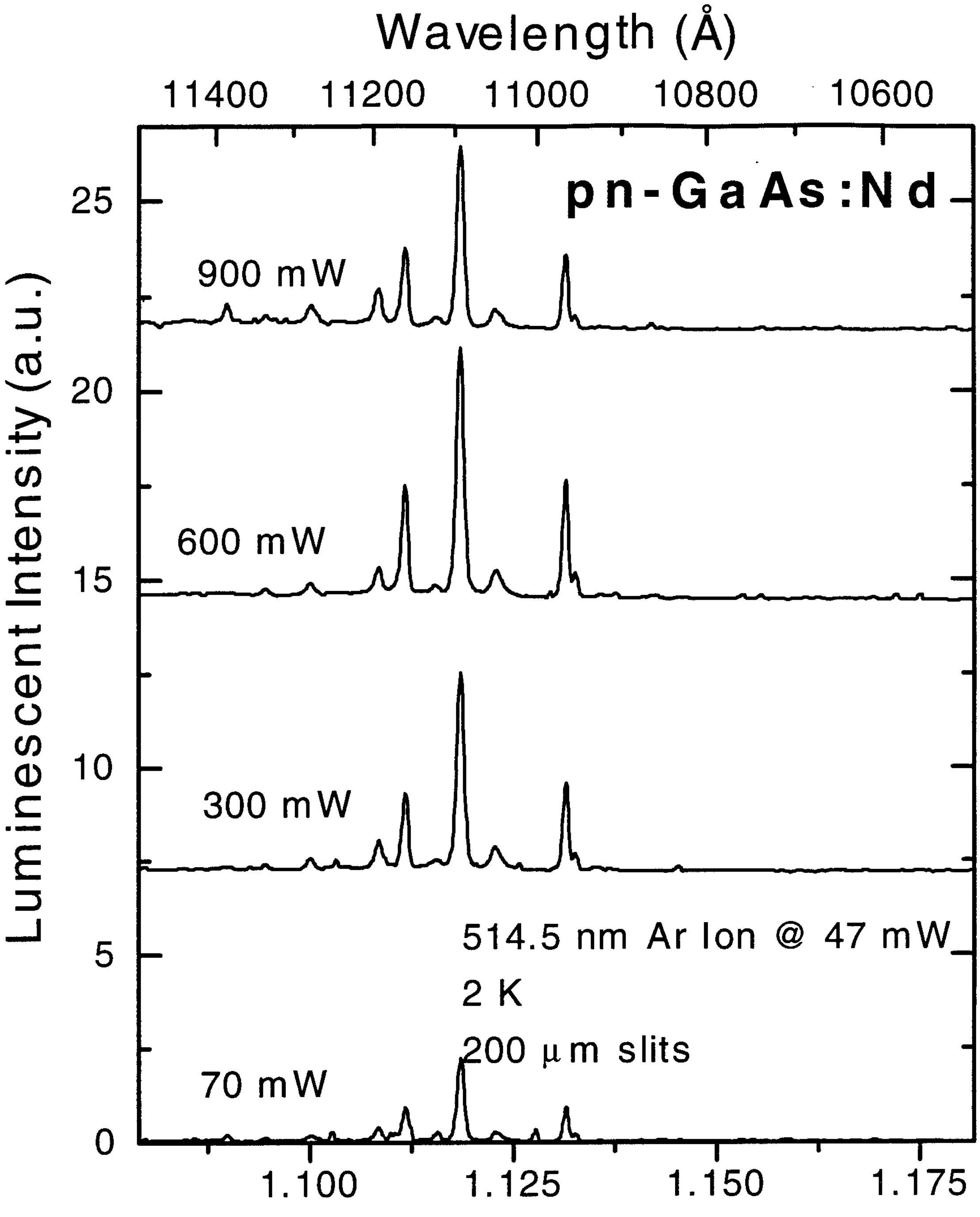

Figure 26. Photoluminescence measured from the pn-GaAs implanted with a Nd at a dose of 5×10^{13} cm^{-2}.

These figures imply that the sample luminescent intensity reaches a saturation limit at around 600 mW input laser power for the unimplanted samples as well as for the implanted samples. However, subsequent measurements using smaller power increments revealed that the saturation limit is in fact closer to 800 mW than 600 mW.

Electroluminescence of RE-implanted GaAs and $Al_xGa_{1-x}As$ pn-Junctions

The EL measurements in general did not show a strong luminescent signal. None of the Er^{3+} implanted samples showed any luminescence and only two of the Nd^{3+} implanted diode packages displayed luminescence. First, a comparison of the electroluminescence of the unimplanted diode packages is presented. Then an ion dose comparison is given for Er^{3+} and Nd^{3+} is made. Finally, an applied voltage study of the Nd^{3+} device that had initially demonstrated EL will be presented. Figure 27 shows the electroluminescent signal produced from the four unimplanted host materials under sufficient applied voltage to draw about ~100 mA through the diode. In the figure, we see that the GaAs and $Al_xGa_{1-x}As$ EL spectra are essentially the same as those from the samples used for PL (they are presented with a reduced amplitude so to fit all four data sets in the same graph). The fact that there are no spectral peaks tells us that we can have confidence that in subsequent implanted sample measurements that none of the spectral peaks observed were due to optically active contaminants present in the host material (this will become important for the Er^{3+} implanted devices).

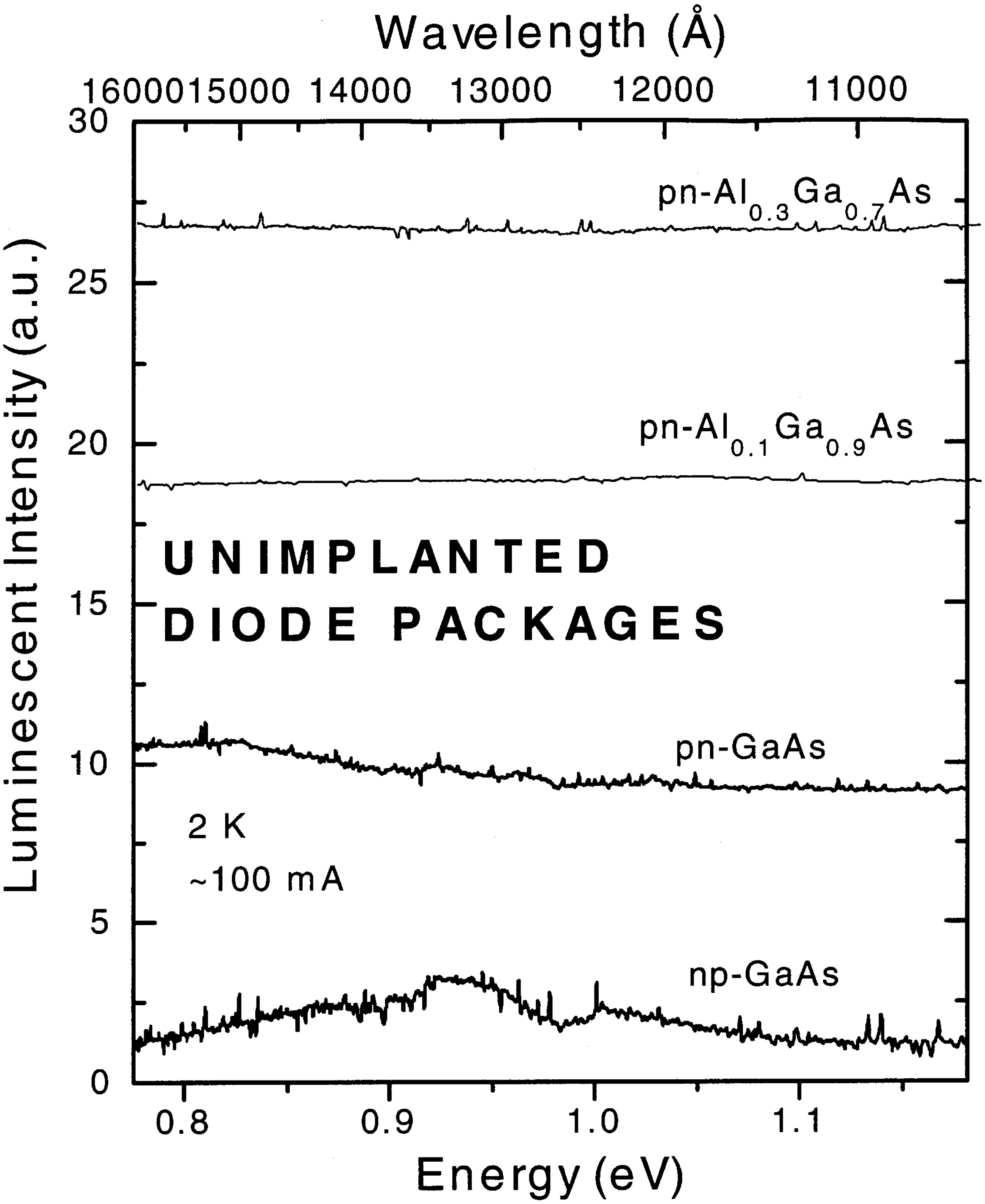

Figure 27. Electroluminescence signal produced from unimplanted diode packages.

Next, a quick overview of the Er^{3+} doped diodes is presented. These results are compared in Figure 28. As before, each diode packages was tested for opens and shorts, and the I-V curve was examined to determine the quality of the diode. All diodes were leaky to some extent. Although no EL was observed from Er ions there appears to be a peak at 1.5303 μm. This peak was found in all samples and its origin is unknown. However, several possibilities as to its origin suggest themselves, such as a lattice damage center or a carbon peak from the p-type material of the diode, but were not investigated.

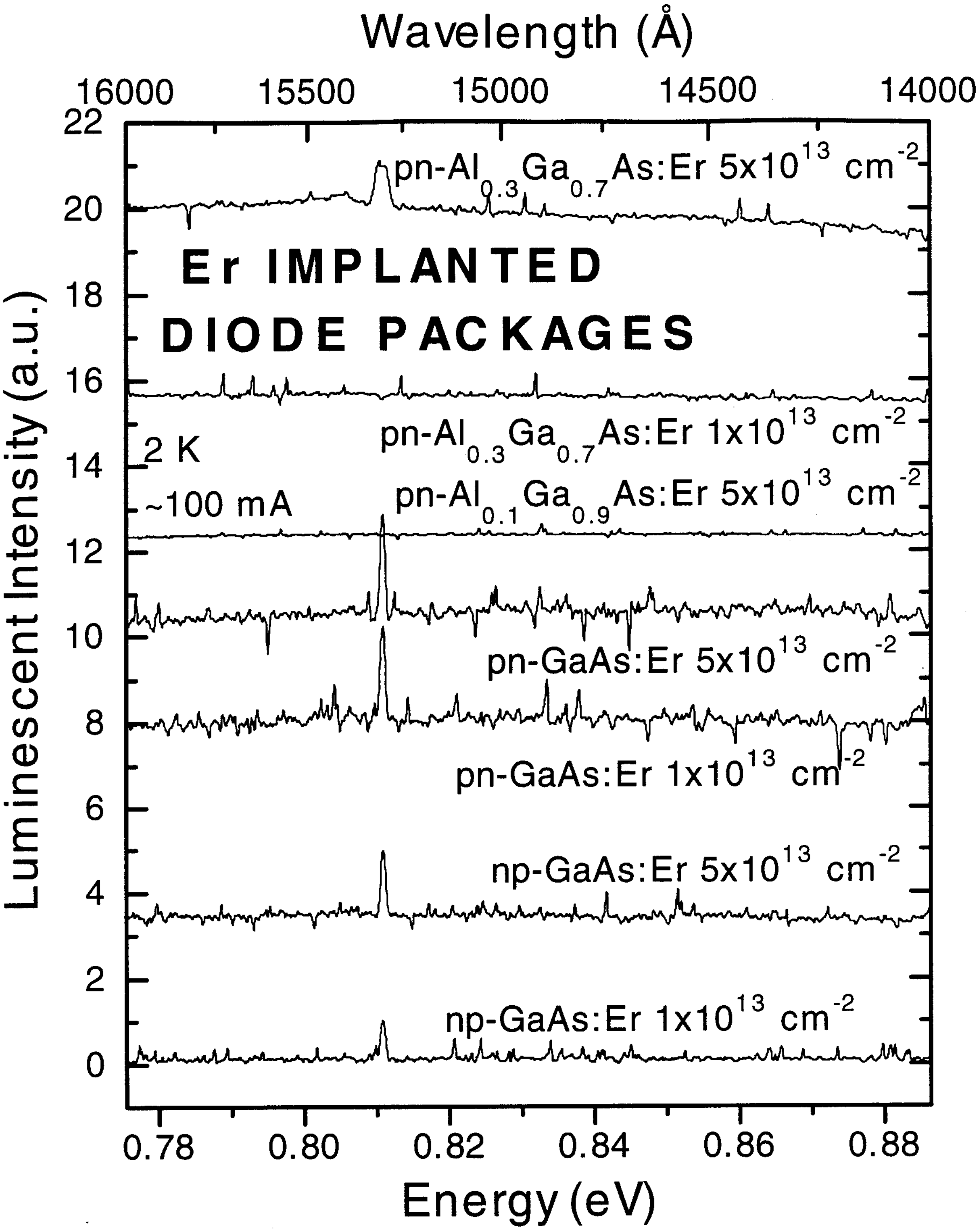

Figure 28. Electroluminescent spectra obtained from Er^{3+} implanted GaAs and $Al_xGa_{1-x}As$ with ion doses of 1×10^{13} and 5×10^{13} cm^{-2}.

The np-GaAs exhibited the 1.5303 μm peak (the luminescent intensity from 5×10^{13} cm^{-2} dose being stronger than that for the 1×10^{13} cm^{-2} dose in all cases), but the strongest intensity came from the pn-GaAs. The $Al_{0.3}Ga_{0.7}As$ sample with Er at a dose of 1×10^{13} cm^{-2} does not exhibit the peak at all, but in the 5×10^{13} cm^{-2} dose, a broadened 1.5303 μm line appears (the 1×10^{13} cm^{-2} dose $Al_{0.1}Ga_{0.9}As$ was lost in the lithography process). This suggests that the Al was quenching the impurity emissions.

The next section provides the results from the Nd^{3+} EL low-temperature measurements. The main reason for the lack of RE^{3+} emission spectra in most $Al_xGa_{1-x}As$ samples is believed to be due to faulty diodes as Nd^{3+} emissions were observed from pn- and np-GaAs at a 1×10^{13} cm^{-2} dose. From the PL measurement results in the previous section, we would expect the emission intensity to increase with dose. However, because no spectral lines were obtained at the higher dose, we can't be sure if the diode was bad or if the dose was too high. The results from the EL measurements are given in Figure 29.

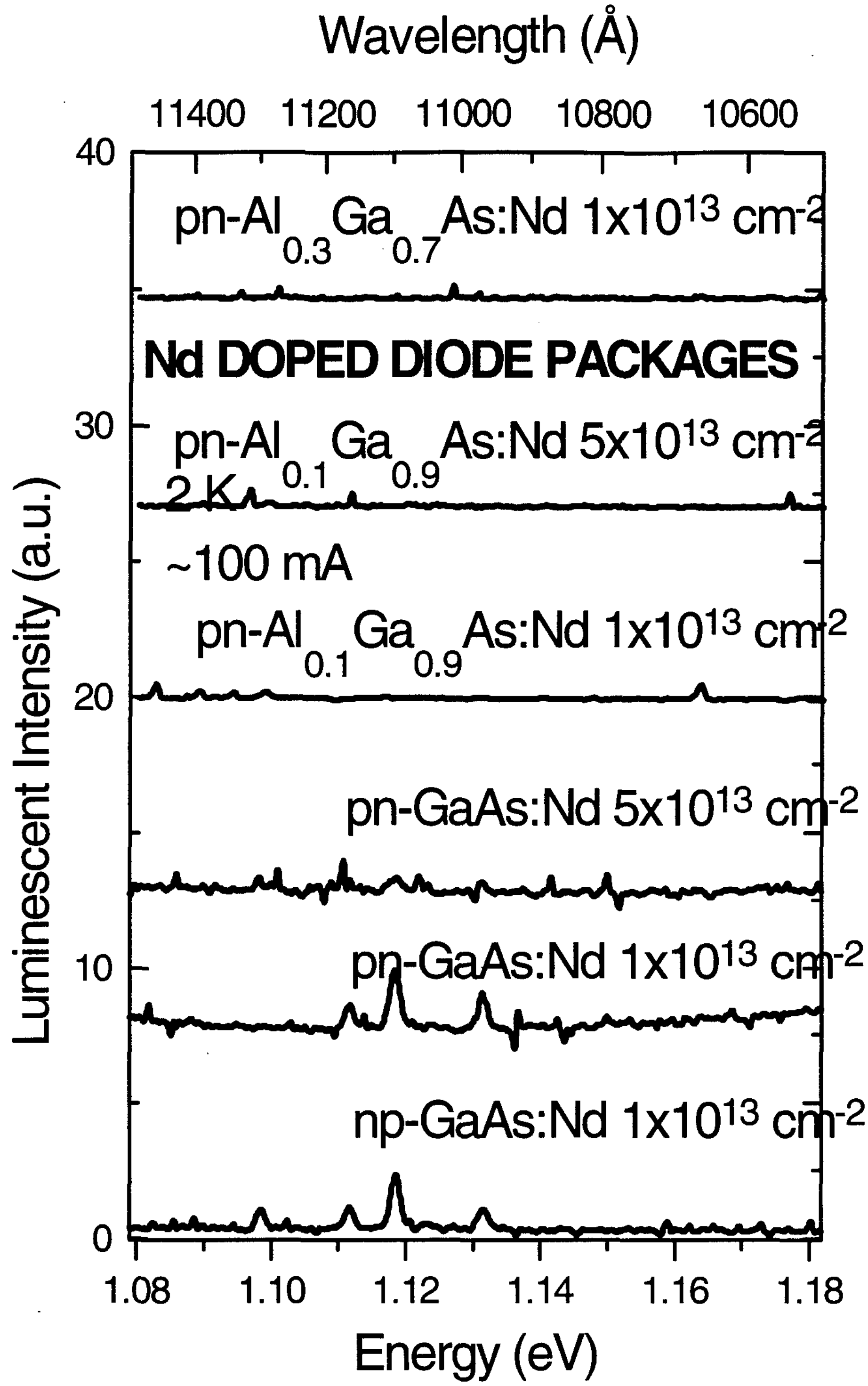

Figure 29. Electroluminescence measurements of Nd^{3+} implanted pn- and np-GaAs and pn-$Al_xGa_{1-x}As$ with ion doses of 1×10^{13} and 5×10^{13} cm^{-2}.

From the above figure, the intra-4f shell emissions of Nd can clearly be seen in both the 1×10^{13} cm^{-2} dose np- and pn-GaAs junctions. There also appears to be a similar group of low intensity peaks in the pn-GaAs package with the 5×10^{13} cm^{-2} dose, however, these peaks are so low as to be on the order of the noise intensity and no confidence can be given to them. A comparison of the position of the ~1.11 eV peak found with EL and PL showed that the two peaks were at the same position as seen in Figure 23 and Figure 29. The rest of the packages did not emit Nd^{3+} luminescence under any circumstances, including varying the applied forward bias and, as a check, the reverse bias. The two packages that did luminesce were set aside for a few days and measured again, this time no luminescence was observed except for an impurity peak at 1130 nm. This impurity peak was not present during the initial np-GaAs measurements. A possible explanation for this occurrence could be that frost forming on the diode after it was removed from the liquid He dewar somehow cracked the diode surface so that a defect luminescent center developed.

V. Conclusions and Recommendations for Future Study

The original goal of this research was the investigation of (a) low temperature PL of the rare earth ER in MOCVD grown Si, and (b) low temperature PL and EL of the rare earths Er and Nd in GaAs and AlGaAs. The PL studies were highly successful. PL was observed from the rare earths in all samples studied. The EL studies were less successful. This lack of success is believed to be primarily due to the quality of the diode structures rather than the quality of the base material or the implants.

Photoluminescence from the MOCVD grown Si:Er^{3+} samples gave the strongest intensity luminescence with samples that were grown with a growth time of 70 minutes and a silane flow rate of 5.0 sccm. Photoluminescence from the ion implanted pn- and np-junctions gave the strongest luminescent intensity for both Er and Nd implanted GaAs pn-junctions with a dose of 5×10^{13} cm^{-2} and a 800 mW laser input power (this was also the power that RE^{3+} luminescence saturated). When the power of the laser was increased to 900 mW, thermal broadening of the peaks became noticeable. For pn-GaAs:Er, some of the smaller peaks were lost in the 1.54 μm peak when a 900 mW laser excitation power was used. Since the Nd peaks are further separated from one another than the Er, this effect was not as noticeable. The aluminum mole fraction variable demonstrated that a 0.1 Al mole fraction in the $Al_xGa_{1-x}As$ produced more photoluminescent intensity than 0.3, but more background noise was also observed for x=0.1 than for x=0.3.

No EL was observed from the GaAs:Er or AlGaAs:Er diode packages. As stated earlier, this lack of luminescence is suspected to have been caused by faulty diodes. EL was observed from GaAs:Nd and AlGaAs:Nd the first time the samples were measured but was not observed on subsequent measurements, again indicating faulty diodes. Samples displaying initial luminescence were pn- and np-junctions with an implanted Nd dose of $1\times10^{13}\,cm^{-2}$ under an applied voltage of 15 V and 19 V, respectively.

Future endeavors involving rare-earth implanted GaAs and $Al_xGa_{1-x}As$ devices, should emphasize the fabrication of quality diode packages. In some cases, the extremely thin contact wires broke and caused a short or open when the slightest pressure was inadvertently applied to them (a puff of air to be exact). Manufacturing more diode packages from which to work with (about 10-20 packages) or making sturdier contacts would help rectify this problem. Another suggestion would be to dice the initial samples into larger pieces. Sample size should be increased from ¼" × ¼" to about 1" × 1". This helps the technician when performing the mesa diode lithography and follows with the suggestion of making more samples.

The topic of oxygen codoping should definitely be explored in future work. Oxygen has been shown to greatly enhance Er and Pr luminescence in n- or p-type $Al_xGa_{1-x}As$ (22). Also Takahei and Taguchi have shown that efficient oxygen incorporation into the lattice occurs with Er present and as a result peak intensities of PL measured samples are 10 times higher than without oxygen codoping (23 and 24). If this enhancement carries over to the pn- and np-junctions, then characterization of luminescent intensity might be performed more easily in PL and may even cause the EL measurements to exhibit the 1.54 μm peak. What effect oxygen codoping with Nd has on luminescent intensity has not been documented. If it did have as great an influence on the luminescence as is does for Er then science would be that much closer to realizing a Nd diode laser.

Of course, a temperature dependent study of the luminescence for both PL and EL of the junctions has not been documented so that would be a possible avenue of research to determine quenching mechanisms. It would be even more feasible if the oxygen codoping actually increased the luminescence.

A laser excitation power study should also be done on the oxygen coimplanted samples to determine when input power begins to thermally broaden the rare-earth peaks to the point where smaller peaks are lost.

Knowing exactly where the ion implantation placed the RE^{3+} would also help in the understanding of what processes are occurring in the EL measurements. A Secondary Ion Mass Spectroscopy (SIMS) of the various ion implanted diodes would be helpful in deciphering data and making future diodes.

A larger range of implant doses should also be considered. Initial work on rare-earth dose in singe n- or p-type material dictated that 5×10^{13} cm^{-2} was the optimum dose. This may not be the case with the junctions. The larger dose material showed the greater intensity. Increasing the dose may also increase the EL signal by providing more rare-earth atoms to be subjected to the electron injection and subsequently an increased amount of radiative transitions might occur.

Bibliography

1. Klein, P., Moore, F. G., and Dietrich H. B. “1.54 μm Electroluminescence in MeV Ion Implanted Er-Doped GaAs,” Electronics Letters. 26 (16): 1299-1300, 2 Aug 1990.

2. Chang, S. J., and Takahei, K., “Studies of GaAs:Er impact excited electroluminescence devices,” Applied Physics Letters. 65 (4): 433-435, 25 Jul 1994.

3. Namavar, Fereydoon. Visible and Infrared (1.54 μm) LED Based on Er-doped Porous Si. AFOSR-TR-FR-60291. Bedford, MA: Spire Corporation, 28 Feb 1994.

4. Thee, Paul L. et al Pr^{3+} luminescence in GaAs and $Al_xGa_{1-x}As$ implanted with Pr (tentative title). Unpublished text. Air Force Institute of Technology, Wright-Patterson AFB, OH, 20 Jun 1995.

5. McKelvey, John P. Solid State Physics: For Engineering and Materials Science. Malabar, FL: Krieger Publishing Company, 1993.

6. Neaman, Donald A. Semiconductor Physics and Devices. Boston: Richard D. Irwin, Inc., 1992.

7. Takahei, K., Taguchi, A., and Horikoshi, Y., “Atomic configuration of the Er-O luminescence center in Er-doped GaAs with oxygen codoping,” Journal of Applied Physics, 76 (7): 4332-4338, 1 Oct 1994.

8. Hengehold, Robert L., Chairman, Advisory Committee. Personal correspondence. Air Force Institute of Technology, Dayton, OH, 8 Nov 1995.

9. Ion Beam Profile Code, version 2.1. Implant Sciences Corporation. 1988.

10. Kozanecki, A., et al “Lattice Location of Erbium Implanted GaAs,” Solid State Communications, 78 (8): 763-766 (1991).

11. Elsaesser, Dave W., et al “Annealing Studies of Er-Implanted GaAs and the Excitation Mechanism of Er in GaAs,” Materials Research Society Symposium, Vol. 301, 1993.

12. DiBartolo, B. Optical Interactions in Solids. New York: John Wiley and Sons, 1968.

13 . Boyn, R., "4f-4f Luminescence of Rare Earth Centers in II-VI Compounds," Physica Status Solidi B. 148(1) New York: VCH Publishers Inc., 1988.

14 . Colon, José E. Luminescence Study of Ion-Implanted and MBE-Grown Er-Doped GaAs and $Al_xGa_{1-x}As$. PhD dissertation. Wright-Patterson AFB, OH: School of Engineering, Air Force Institute of Technology, Mar 1993. (AAJ-6948)

15 . Thee, Paul L. The Excitation Mechanism of Praseodymium-Doped Semiconductors. PhD dissertation. Wright-Patterson AFB, OH. School of Engineering, Air Force Institute of Technology, Jun 1994.

16 . Nakagome, Hiroshi and Kenichiro Takahei, "MOCVD Growth and PL-Characteristics of Nd Doped GaAs," Japanese Journal of Applied Physics, 28 (11): 2098-2100, Nov 1989.

17 . Sze, S. M., Semiconductor Devices: Physics and Technology. New York: John Wiley and Sons, 1985.

18 . Zambuto, Mauro, Semiconductor Devices. New York: McGraw-Hill Book Company, 1989.

19 . Pankove, J. I., "Introduction," Topics in Applied Physics, Vol. 17: Electroluminescence. edited by J. I. Pankove. Berlin: Springer-Verlag, 1977.

20 . North Coast Scientific Corporation. Santa Rosa, CA. Jan 1978.

21 . Boyd, Robert W., Radiometry and the Detection of Optical Radiation. New York: John Wiley and Sons, 1983.

22 . Colon, Jose E., et al "Enhancement of the Er^{3+} emissions from AlGaAs:Er codoped with oxygen," Applied Physics Letters, 63 (2): 216-218 (12 Jul 1993).

23 . Takahei, Kenichiro and Taguchi, Akihito, "Selective formation of an efficient Er-O luminescence center in GaAs by metalorganic chemical vapor deposition under an atmosphere containing oxygen," Journal of Applied Physics. 74 (3): 1979-1982 (1 Aug 1993).

24 . Takahei, Kenichiro and Taguchi, Akihito, "Efficient Er Luminescence Centers Formed in GaAs by Metalorganic Chemical Vapor Deposition with Oxygen Codoping," Japanese Journal of Applied Physics Vol. (33). Part 1, No. 1B: 709-711 (Jan 1994).

Vita

First Lieutenant James R. Hunter [redacted] He spent most of his years with his parents Shirley and Robert Hunter in the small town of Athol, Massachusetts aspiring to be a great writer. He graduated from Athol High School in 1988 and entered the USAF Academy in Colorado Springs, Colorado. There, his dreams of being a writer were dashed upon the Rockies and physics became his new career calling. After graduating from the Academy in 1992 with a Bachelor of Science Degree in Physics, he spent the next two years at the Technical Operations Division at McClellan AFB, Sacramento, California. There he worked as the Chief of Nuclear Quality Assurance performing managerial duties and organizing a uranium foil irradiation for the benefit of AFTAC. In May 1994, he entered the School of Engineering of the Air Force Institute of Technology to pursue a Master's of Science in Engineering Physics.

[redacted]

REPORT DOCUMENTATION PAGE

Form Approved
OMB No. 0704-0188

1. AGENCY USE ONLY *(Leave blank)*

2. REPORT DATE
December 1996

3. REPORT TYPE AND DATES COVERED
Master's Thesis

4. TITLE AND SUBTITLE
Photoluminescence and Electroluminescence of Erbium and Neodymium Implanted Semiconductors

5. FUNDING NUMBERS

6. AUTHOR(S)
James R. Hunter, 1st Lt, USAF

7. PERFORMING ORGANIZATION NAME(S) AND ADDRESS(ES)
Air Force Institute of Technology, WPAFB OH 45433-6583
Robert L. Hengehold

8. PERFORMING ORGANIZATION REPORT NUMBER
AFIT/GAP/ENP/95D-09

9. SPONSORING / MONITORING AGENCY NAME(S) AND ADDRESS(ES)
Gernot S. Pomrenke
AFOSR/NE (Bldg 410)
Bolling AFB, Washington D.C. 20332-6448

10. SPONSORING / MONITORING AGENCY REPORT NUMBER

11. SUPPLEMENTARY NOTES

12a. DISTRIBUTION / AVAILABILITY STATEMENT
Approved for public release; distribution unlimited

12b. DISTRIBUTION CODE

13. ABSTRACT *(Maximum 200 words)*

Luminescent experiments were used to study conditions for excitation of the rare earths, erbium and neodymium, in ion-implanted and MOCVD grown GaAs and ion implanted $Al_xGa_{1-x}As$ (x=0.1, 0.3). Low temperature photoluminescence (PL) and electroluminescence (EL) using forward bias only were the two experimental techniques utilized. The rare earth emissions were observed as a function of dopant concentration, aluminum mole fraction, laser excitation power, and applied voltage. Photoluminescence of the MOCVD grown samples resulted in the strongest intensity luminescence from samples grown in 70 minutes time with hydrogen present. Photoluminescence of the ion implanted pn junctions revealed that with a dose of $5x10^{13}$ cm^{-2} and with a peak dopant concentration in the p type region produced the highest luminescent intensity. An aluminum mole fraction of 0.1 showed more intensity than 0.3, however, more background noise was also observed. Peak luminescent intensity was observed with an input power of ~600 mW for both Er and Nd. Electroluminescence of the ion implanted samples showed some Nd under an applied forward voltake of 15 V.

14. SUBJECT TERMS
Photoluminescence, Electroluminescence, Erbium, Neodymium, Semiconductors, Ion Implantation, MOCVD

15. NUMBER OF PAGES
64

16. PRICE CODE

17. SECURITY CLASSIFICATION OF REPORT
Unclassified

18. SECURITY CLASSIFICATION OF THIS PAGE
Unclassified

19. SECURITY CLASSIFICATION OF ABSTRACT
Unclassified

20. LIMITATION OF ABSTRACT
UL